BIT manuscript No.
(will be inserted by the editor)

Dirichlet-Neumann Waveform Relaxation Methods for Parabolic and Hyperbolic Problems in Multiple Subdomains

Martin J. Gander · Felix Kwok · Bankim C. Mandal

Received: July 7, 2020/ Accepted: date

Abstract In this paper, a new waveform relaxation variant of the Dirichlet-Neumann algorithm is introduced for general parabolic problems as well as for the second-order wave equation for decompositions with multiple subdomains. The method is based on a non-overlapping decomposition of the domain in space, and the iteration involves subdomain solves in space-time with transmission conditions of Dirichlet and Neumann type to exchange information between neighboring subdomains. Regarding the convergence of the algorithm, two main results are obtained when the time window is finite: for the heat equation, the method converges superlinearly, whereas for the wave equation, it converges after a finite number of iterations. The analysis is based on Fourier-Laplace transforms and detailed kernel estimates, which reveals the precise dependence of the convergence on the size of the subdomains and the time window length. Numerical experiments are presented to illustrate the performance of the algorithm and to compare its convergence behaviour with classical and optimized Schwarz Waveform Relaxation methods. Experiments involving heterogeneous coefficients and non-matching time grids, which are not covered by the theory, are also presented.

AMS subject classifications: 65M55, 65Y05, 65M15

Keywords Dirichlet-Neumann · Waveform Relaxation · Heat equation · Wave equation · Domain decomposition.

Martin J. Gander
Department of Mathematics, University of Geneva, Switzerland
E-mail: martin.gander@unige.ch

Felix Kwok
Department of Mathematics, Hong Kong Baptist University, Hong Kong
E-mail: felix_kwok@hkbu.edu.hk

Bankim C. Mandal
School of Basic Sciences (Mathematics), Indian Institute of Technology Bhubaneswar, India
E-mail: bmandal@iitbbs.ac.in

1 Introduction

Recently, the Dirichlet-Neumann Waveform Relaxation (DNWR) method has been proposed in [37,20,21] to solve evolution problems in space-time on parallel computers. The method is based on a non-overlapping decomposition of the domain in space and the time interval into time windows, and the iteration requires subdomain solves with Dirichlet boundary conditions followed by subdomain solves with Neumann boundary conditions. The DNWR method can be derived by formally extending the elliptic Dirichlet–Neumann (DN) method of [3] to time dependent problems (see also [6], [39] and [40] for a few variants of the DN method). Indeed, such an approach has been used to derive other Waveform Relaxation (WR) methods, such as the overlapping Schwarz WR method in [22,24], where its convergence is also analyzed for parabolic problems. A variant with optimized transmission conditions has also been proposed and analyzed in [15,2,1] for parabolic and [16,14] for hyperbolic problems.

For elliptic problems, the convergence of the DN algorithm is now well understood, see for example the book [48] and references therein. There are also estimates available when subdomain problems are solved inexactly, see [4]. For the time-dependent diffusion equation, a first analysis for two-subdomain decompositions already appeared in [33,34], where the DNWR method was presented not in its own right, but rather as a comparison to a Robin-Robin type method introduced in that article. The analysis presented there, which is based on a Fourier decomposition in time, does not allow one to prove superlinear convergence, which is nonetheless typical for waveform relaxation methods. The first superlinear convergence result for the 1D heat equation was proved in [20,37] using the Laplace transform technique; the same technique also allows one to prove finite step convergence for the 1D wave equation for two subdomains, see [21].

The DN and DNWR methods have applications beyond the heat and wave equations. For advection-diffusion problems, the DN method is shown to have superior performance over the more symmetric NN method if one chooses the transmission conditions carefully depending on the direction of flow; for more details, see [7], where a Robin variant has also been proposed, which then becomes very efficient for advection-dominated cases. The DN algorithm has also been used to solve heterogeneous problems, such as contact problems [30], Stokes-Darcy coupling [10] and high contrast dense composites [25]. The DN method has also been used as a subroutine for the snapshot generation within a reduced basis method, see [35] for the method description and [41] for error estimates. The recently invented multitrace formulation for scattering problems [8,26] also naturally leads to the DN method when a block iteration is used, see [11]. For time-dependent problems, the DN method has been applied to nonlinear systems arising from the time discretization of a thermal fluid-structure interaction problem in [42]. In that paper, the authors also showed for the special case of a heat equation that the contraction factor of the method decreases to zero as the time step is refined. For the heat equation with heterogeneous coefficients, the authors also proved a similar asymptotic result in [44] for the closely related Neumann–Neumann Waveform Relaxation (NNWR) method, which has been derived independently in [31] and in [27,28] based on the Neumann-Neumann method

for elliptic problems in [5,9,32]. An analysis of NNWR for the heat and wave equations can be found in [38,36]. More applications and analysis of NNWR methods, when applied to heterogeneous coupled heat equations and to thermal fluid-structure interaction problems, can be found in [43,45].

Since DNWR can use only one processor in the two-subdomain case, it is not a parallel method in practice; a decomposition into many subdomains is needed in order for the method to become a useful parallel solver. We present here a general DNWR for the many-subdomain case and general parabolic and hyperbolic problems, and give a detailed convergence analysis when the algorithm is applied to one dimensional heat and wave equations. We then extend our convergence results also to the case of two dimensional wave equations. To further increase parallelism, a technique recently introduced in [47] can be used, which allows the concurrent execution of several WR iterations on different time blocks without changing the convergence behavior of WR. Such an implementation of DNWR then leads to a fully space-time parallel method on many processors. Note that there are other ways to obtain parallelism in time in WR methods: see [29] for the coupling of DNWR and NNWR to parareal methods. For more on parallel-in-time integration, see [13] and references therein.

We consider two PDEs on a bounded domain $\Omega \subset \mathbb{R}^n, 0 < t < T$, $n = 1,2,3$, with a smooth boundary as our guiding examples: the linear parabolic diffusion problem

$$\begin{aligned} \mathscr{L}_d(u) := \tfrac{\partial u}{\partial t} - \nabla \cdot (\kappa(x,t)\nabla u) &= f(x,t),\ x \in \Omega,\ 0 < t < T, \\ u(x,0) &= u_0(x),\ \ x \in \Omega, \\ u(x,t) &= g(x,t),\ x \in \partial\Omega,\ 0 < t < T, \end{aligned} \tag{1.1}$$

where $\kappa(x,t) \geq \kappa_0 > 0$, and the hyperbolic wave propagation problem

$$\begin{aligned} \mathscr{L}_w(u) := \tfrac{\partial^2 u}{\partial t^2} - c^2(x)\Delta u &= f(x,t),\ x \in \Omega, 0 < t < T, \\ u(x,0) &= u_0(x),\ \ x \in \Omega, \\ u_t(x,0) &= v_0(x),\ \ x \in \Omega, \\ u(x,t) &= g(x,t),\ x \in \partial\Omega, 0 < t < T, \end{aligned} \tag{1.2}$$

with $c(x) \geq c_0 > 0$ being a positive function.

We introduce in Section 2 the DNWR algorithm with multiple subdomains, and explain why a certain scheduling for the subdomain solves is needed to make the DNWR algorithm well defined. We then formulate in Subsection 2.1 the DNWR algorithm for parabolic problems of the form (1.1) and a sequential domain decomposition into many subdomains, and state our first main convergence result, namely superlinear convergence in the special case of the one dimensional heat equation in Subsection 2.2. In Subsection 2.3 we present the DNWR algorithm for the wave equation (1.2), and give our second main convergence result, namely convergence in a finite number of steps in Subsection 2.4. The technical tools and convergence analyses are presented in Section 3. To illustrate our analysis, we show numerical results in Section 4, where we also explore the behavior of DNWR in configurations not covered by our analysis.

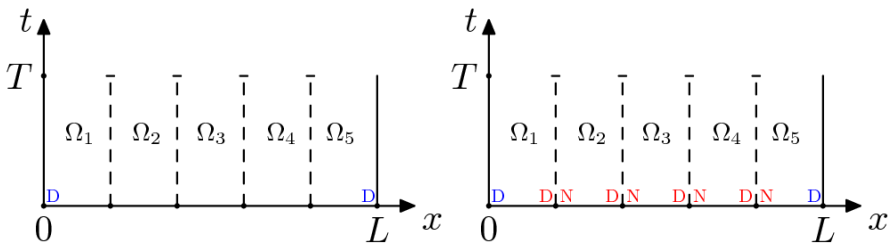

Fig. 2.1: Left: example of a non-overlapping decomposition of the domain into $N = 5$ subdomains. Right: arrangement of the DNWR transmission conditions following A1

2 The Dirichlet Neumann Waveform Relaxation Method

Assume that we have a general decomposition of the spatial domain Ω into non-overlapping subdomains Ω_j, $j = 1,2,\ldots,N$, and interfaces Γ_{ij} between subdomains Ω_i and Ω_j. The DNWR algorithm for this domain decomposition and a general operator $\mathscr{L}$, which can either be the diffusion operator $\mathscr{L}_d$ defined in (1.1) or the wave operator $\mathscr{L}_w$ defined in (1.2), solves for $k = 1,2,\ldots$ [1]

$$\begin{aligned}
\mathscr{L}(u_i^k) &= f, && \text{in } \Omega_i \times (0,T),\\
u_i^k &= w_{ij}^k, && \text{on } \Gamma_{ij}, \text{ if } D_{ij} = i,\\
\partial_{n_i} u_i^k &= \partial_{n_i} u_j^k, && \text{on } \Gamma_{ij}, \text{ if } D_{ij} = j,\\
w_{ij}^k &= \theta u_{[D]_{ij}}^k + (1-\theta) w_{ij}^{k-1} && \text{on } \Gamma_{ij},
\end{aligned} \tag{2.1}$$

where $D_{ij} = i$ means that u_i takes Dirichlet data along the interface Γ_{ij}, and u_j takes Neumann Data, and $D_{ij} = j$ means the opposite, and $[D]_{ij} = j$ if $D_{ij} = i$ and vice versa. To start the DNWR algorithm, we need an initial guess w_{ij}^0 on the interfaces Γ_{ij}.

Note that this algorithm implies a specific data dependence in the computation, since in the Dirichlet-Neumann method, one has to first do the Dirichlet solves, before the data required for the Neumann solves become available. In fact, if $D_{ij} \neq i$, then the solution u_i^k on subdomain Ω_i cannot be computed until u_j^k has been computed. One can thus define a dependency graph for the algorithm: consider the directed graph $G = (V,E)$, with vertices $V = \{1,\ldots,N\}$ and edges $E = \{(i,j) : D_{ij} = i\}$. This dependency graph allows us to see when the algorithm is well-defined: this is the case if and only if G is acyclic, because only then the algorithm can actually be run. To illustrate this, we consider a 1D example: suppose the spatial domain $\Omega := (0,L)$ is decomposed into N non-overlapping subdomains $\Omega_j = (x_{j-1}, x_j)$, $j = 1,\ldots,N$, as shown in Figure 2.1 on the left. One can then, for example, impose the Dirichlet and Neumann transmission conditions along the interfaces in three different arrangements:

(A1) the Dirichlet data is always used by the subdomain on the left, i.e., $D_{j,j+1} = j$.

[1] For simplicity, we do not explicitly write the initial and boundary conditions coming from the underlying equation.

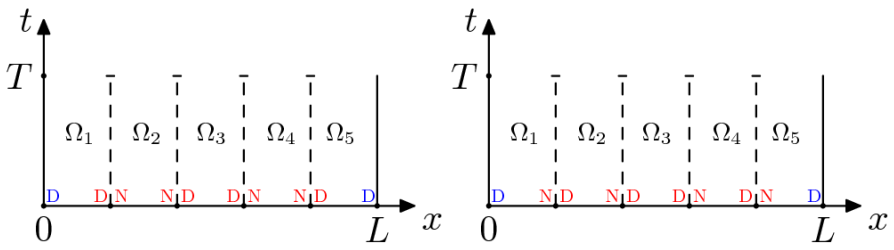

Fig. 2.2: Two further arrangements of the DNWR transmission conditions: A2 on the left, and A3 on the right

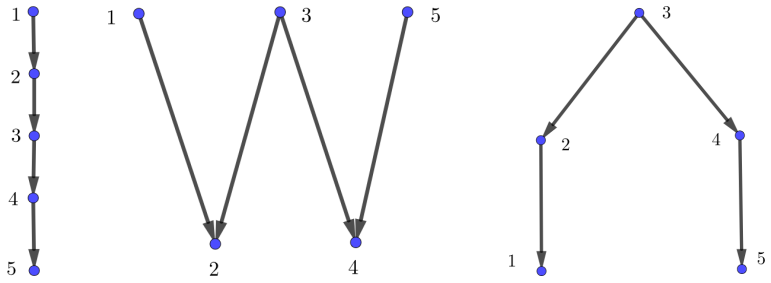

Fig. 2.3: Dependency graphs corresponding to three arrangements A1, A2 and A3 with five subdomains

(A2) the Dirichlet data is always used by the subdomain with odd index, i.e., $D_{i,i+1} = i$ if i is odd, and $D_{i,i+1} = i+1$ otherwise. If N is even, $D_{N-1,N} = N-1$ and a Dirichlet condition is used along the rightmost physical boundary.

(A3) the Dirichlet data is used by the subdomain closest to the middle of the domain, i.e., $D_{i,i+1} = i$ if $i > \lfloor N/2 \rfloor$, and $D_{i,i+1} = i+1$ otherwise.

Figures 2.1 and 2.2 illustrate the three arrangements when $N = 5$. The letter D in blue denotes the Dirichlet boundary condition along the two physical boundaries, and D and N in red denote the Dirichlet and Neumann transmission conditions along the subdomain interfaces. From the corresponding dependency graphs G shown in Figure 2.3, we see that in each case, G is acyclic, so the corresponding DNWR algorithm is well defined: in the first case, A1, one would have to solve sequentially from the first to the last subdomain, and thus has no parallelism without using further pipelining techniques. In the case A2, one could first solve in parallel on Ω_1, Ω_3 and Ω_5, followed by solving in parallel on Ω_2 and Ω_4, and in the case of A3, one would have to start in the middle solving on Ω_3, following by solving in parallel on Ω_2 and Ω_4, and then in parallel on Ω_1 and Ω_5. The arrangement A2 is known as a *red-black ordering* of the subdomains, whereas A3 is an arrangement first proposed in [12] for generalizing the Dirichlet-Neumann method to multiple subdomains.

To illustrate the convergence behavior of the DNWR algorithm with these different arrangements, we discretize (2.1) for the case of the heat equation in 1D (see Section 2.1 for more details) using standard centered finite differences in space and

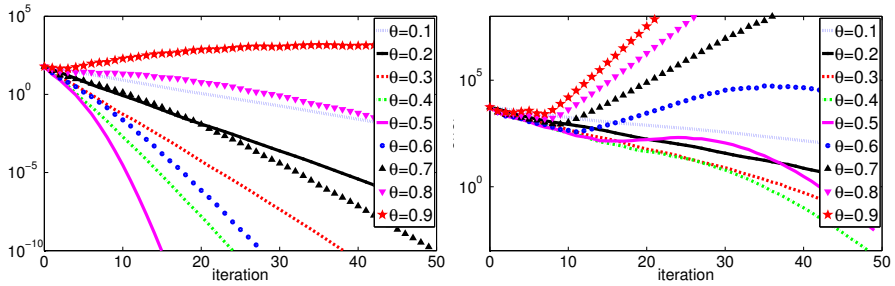

Fig. 2.4: Arrangement A1: Convergence of multi-subdomain DNWR for the heat equation for different values of θ, on the left for $T = 2$ and on the right for $T = 20$

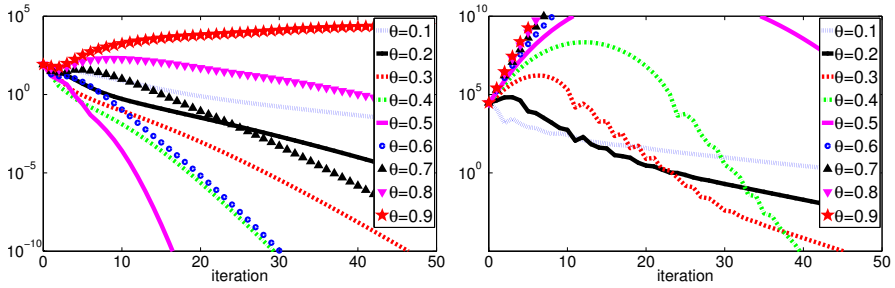

Fig. 2.5: Arrangement A2: Convergence of multi-subdomain DNWR for the heat equation for different values of θ, on the left for $T = 2$ and on the right for $T = 20$

backward Euler in time, and run the DNWR algorithm numerically for different time window sizes and relaxation parameters. We use $u_0(x) = 0$, $g(x,t) = (x+1)t$, and for the initial guess $w_i^0(t) = t^2, t \in [0,T]$. We show in Figure 2.4 for the arrangement A1 the convergence curves for different values of the relaxation parameter θ. We see that the algorithm seems to converge superlinearly, that convergence over the short time interval is much better than over the long time interval[2] (note the different scale), and that there seems to exist an optimal relaxation parameter θ which leads to best performance. We next show in Figure 2.5 the corresponding results for the arrangement A2, and in Figure 2.6 the results for the arrangement A3. We see that the convergence behavior of DNWR with the three arrangements A1, A2 and A3 is similar for smaller time windows, but for longer time windows, the arrangement A3 leads to much faster convergence in terms of the number of iterations. Although the dependency graph of A3 suggests that half of the subdomain solves must be done sequentially, it is actually possible to use up to $\lceil N/2 \rceil$ processors in parallel, just like for the arrangement A2. In fact, it was shown in [47] that the pipelining technique can be applied to the arrangement A3 to use more processors: an example is shown in Figure 2.7, where iterates shown in different colours in the same row can be computed in parallel using

[2] This indicates that one should cut long time intervals into shorter time windows and then apply the algorithm time window by time window, like in most WR methods

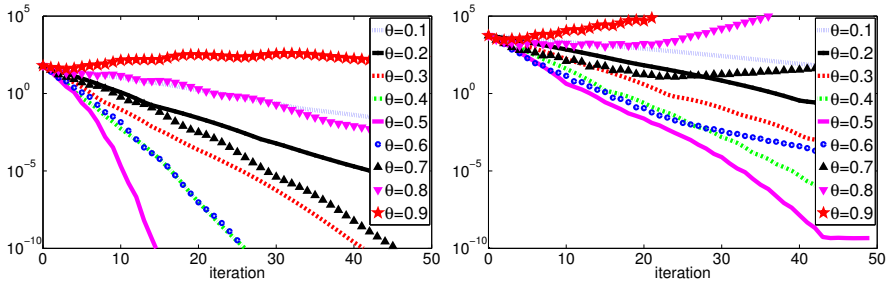

Fig. 2.6: Arrangement A3: Convergence of multi-subdomain DNWR for the heat equation for different values of θ, on the left for $T = 2$ and on the right for $T = 20$

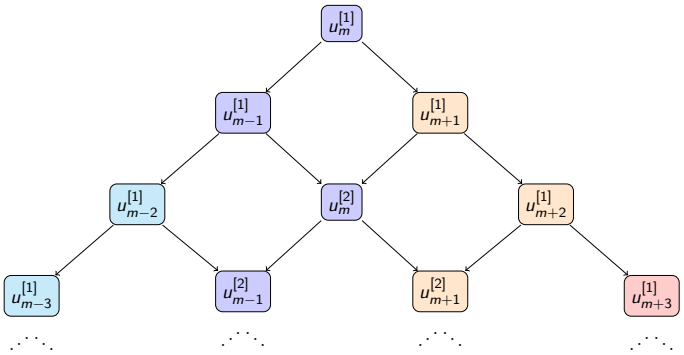

Fig. 2.7: Parallel computation of DNWR iterates for the arrangement A3.

different processors. Given its better convergence behaviour and the ability to utilize many processors in parallel, we will focus on the arrangement A3 when analyzing DNWR algorithms in the remainder of the article, although we will also show the behaviour of DNWR for the wave equation for the other arrangements in our numerical experiments.

2.1 DNWR for Parabolic Problems

We now define the DNWR method for the parabolic model problem (1.1) on the space-time domain $\Omega \times (0,T)$ with Dirichlet boundary conditions on $\partial\Omega$. Suppose the spatial domain Ω is partitioned into N non-overlapping subdomains $\Omega_i, i = 1,\ldots,N$ without any cross-points, as illustrated in Figure 2.8. We denote by u_i the restriction of the solution u of (1.1) to Ω_i. For $i = 1,\ldots,N-1$, set $\Gamma_i := \partial\Omega_i \cap \partial\Omega_{i+1}$. We further define $\Gamma_0 = \Gamma_N = \emptyset$. We denote by $n_{i,i-1}$ and $n_{i,i+1}$ the unit outward normal for Ω_i on the interface $\Gamma_j, j = i-1, i$ (for Ω_1, Ω_N we have only $n_{1,2}$ and $n_{N,N-1}$ respectively). In

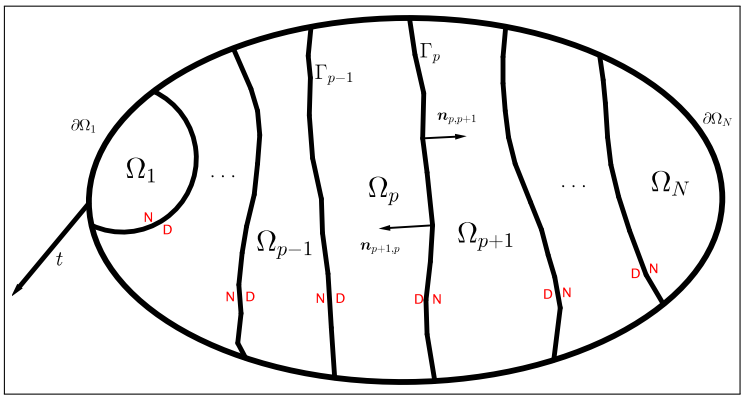

Fig. 2.8: Domain decomposition into many non-overlapping strip-like subdomains

Figure 2.8, D and N in red denote the Dirichlet and Neumann transmission conditions along the interfaces as in arrangement A3.

The DNWR algorithm starts with an initial guess for the Dirichlet traces $w_i^0(x,t)$ along the interfaces $\Gamma_i \times (0,T)$, $i = 1,\ldots,N-1$, and picking the middle subdomain Ω_p for $p = \lceil N/2 \rceil$ to start according to arrangement A3. The DNWR algorithm then performs for $k = 1,2,\ldots$ the following computation: it solves

$$\begin{aligned} \partial_t u_p^k - \nabla\cdot\left(\kappa(x,t)\nabla u_p^k\right) &= f, && \text{in } \Omega_p, \\ u_p^k &= g, && \text{on } \partial\Omega\cap\partial\Omega_p, \\ u_p^k &= w_i^{k-1}, && \text{on } \Gamma_i, i = p-1, p, \end{aligned} \tag{2.2}$$

and then for $\ell = 1,2,\ldots,p-1$, it solves for $i = p-\ell$ and $j = p+\ell$ (continue until $j = N$ for even N)

$$\begin{aligned} \partial_t u_i^k &= \nabla\cdot\left(\kappa(x,t)\nabla u_i^k\right) + f, && \text{in } \Omega_i, \\ u_i^k &= w_{i-1}^{k-1}, && \text{on } \Gamma_{i-1}, \\ \partial_{n_{i,i+1}} u_i^k &= -\partial_{n_{i+1,i}} u_{i+1}^k, && \text{on } \Gamma_i, \\ u_i^k &= g, && \text{on } \partial\Omega\cap\partial\Omega_i, \end{aligned} \qquad \begin{aligned} \partial_t u_j^k &= \nabla\cdot\left(\kappa(x,t)\nabla u_j^k\right) + f, && \text{in } \Omega_j, \\ \partial_{n_{j,j-1}} u_j^k &= -\partial_{n_{j-1,j}} u_{j-1}^k, && \text{on } \Gamma_{j-1}, \\ u_j^k &= w_j^{k-1}, && \text{on } \Gamma_j, \\ u_j^k &= g, && \text{on } \partial\Omega\cap\partial\Omega_j, \end{aligned} \tag{2.3}$$

and the interface data is updated via

$$\begin{aligned} w_i^k(x,t) &= \theta u_i^k\big|_{\Gamma_i\times(0,T)} + (1-\theta) w_i^{k-1}(x,t),\ 1 \le i < p, \\ w_j^k(x,t) &= \theta u_{j+1}^k\Big|_{\Gamma_j\times(0,T)} + (1-\theta) w_j^{k-1}(x,t),\ p \le j \le N-1, \end{aligned} \tag{2.4}$$

for some parameter $\theta \in (0,1]$.

Note that the outer loop in k in the above algorithm need not be completely sequential, since the subdomain solves for different k can be computed simultaneously in a pipeline fashion in order to obtain more parallelism: see Figure 2.7 and [47] for details. However, since the precise scheduling of the computing tasks will not affect the mathematical properties of the algorithm, we will simply use this version of the algorithm for analysis purposes in the remainder of the paper.

2.2 DNWR Convergence Estimate for the Heat Equation

We next present our convergence estimate of the DNWR algorithm (2.2)–(2.3)–(2.4) for the specific case of the 1D heat equation with $\kappa(x,t) = \nu$. The decomposition of the domain $\Omega := (0,L)$ is thus into N non-overlapping subdomains $\Omega_i := (x_{i-1}, x_i)$, $i = 1,\dots,N$, with subdomain length $h_i := x_i - x_{i-1}$. The physical boundary conditions are $u(0,t) = g_0(t)$ and $u(L,t) = g_L(t)$, and since we will study the error equations, by linearity we can consider $f(x,t) = 0$, $u_0(x) = 0$, and $g_0(t) = g_L(t) = 0 = u_0(x)$. We take $\{w_i^0(t)\}_{i=1}^{N-1}$ as initial guesses along the interfaces $\{x = x_i\} \times (0,T)$, and have from the physical boundaries $w_0^k(t) = w_N^k(t) = 0$ for all k. Denoting by $\{z_i^k(t)\}_{i=1}^{N-1}$ for $k = 1,2\dots$ the Neumann traces along the interfaces, we compute

$$\begin{aligned} \partial_t u_p^k - \nu \partial_{xx} u_p^k &= 0, \qquad x \in \Omega_p, \\ u_p^k(x_{p-1},t) &= w_{p-1}^{k-1}(t), \\ u_p^k(x_p,t) &= w_p^{k-1}(t) \end{aligned} \tag{2.5}$$

for $p = \lceil N/2 \rceil$ and then for $\ell = 1,2,\dots,p-1$ we solve in parallel for $i = p - \ell$ and $j = p + \ell$ (continue until $j = N$ for even N)

$$\begin{aligned} &\partial_t u_i^k - \nu \partial_{xx} u_i^k = 0, \qquad x \in \Omega_i, \\ &u_i^k(x_{i-1},t) = w_{i-1}^{k-1}(t), \\ &\partial_x u_i^k(x_i,t) = z_i^k(t), \end{aligned} \qquad \begin{aligned} &\partial_t u_j^k - \nu \partial_{xx} u_j^k = 0, \qquad x \in \Omega_j, \\ &-\partial_x u_j^k(x_{j-1},t) = z_{j-1}^k(t), \\ &u_j^k(x_j,t) = w_j^{k-1}(t), \end{aligned} \tag{2.6}$$

and the interface data is updated with the parameter $\theta \in (0,1]$ via

$$\begin{aligned} w_i^k(t) &= \theta u_i^k(x_i,t) + (1-\theta) w_i^{k-1}(t), \quad z_i^k(t) = \partial_x u_{i+1}^k(x_i,t), \ 1 \le i < p, \\ w_j^k(t) &= \theta u_{j+1}^k(x_j,t) + (1-\theta) w_j^{k-1}(t), \ z_j^k(t) = -\partial_x u_j^k(x_j,t), \ p \le j \le N-1. \end{aligned} \tag{2.7}$$

The ultimate goal of our analysis is to understand how the error $w_i^k(x,t)$ converges to zero as $k \to \infty$. We have the following main convergence result for DNWR for the heat equation; the proof of this result will be given in Subsection 3.2.

Theorem 2.1 (Convergence of DNWR for the heat equation) *For $\theta = 1/2$ and $T > 0$ fixed, the DNWR algorithm for the arrangement (A3), defined in (2.5)–(2.7) for $N(>2)$ subdomains of unequal sizes $h_i, 1 \le i \le N$ converges superlinearly with the estimate*

$$\max_{1 \le i \le N-1} \| w_i^k \|_{L^\infty(0,T)} \le \left(N - 2 + \frac{2h_{\max}}{h_p} \right)^k \operatorname{erfc}\left(\frac{k h_{\min}}{2\sqrt{\nu T}} \right) \max_{1 \le i \le N-1} \| w_i^0 \|_{L^\infty(0,T)},$$

where $p = \lceil N/2 \rceil$, $h_{\max} := \max_{1 \le i \le N} h_i$ and $h_{\min} := \min_{1 \le i \le N} h_i$.

A sharper bound can be deduced in case of equal subdomains; see Appendix A at the end. Note that the choice $\theta = 1/2$ is the reason behind superlinear convergence; all other choices lead to linear convergence, even in the two-subdomain case, see [20].

2.3 DNWR for the Wave Equation

We use the same geometric configuration and sequential domain decomposition as in the parabolic case in Subsection 2.1, and also the subdomain solve arrangement A3, even though other arrangements could be considered as well. With $p := \lceil N/2 \rceil$, and given initial Dirichlet traces $w_i^0(x,t)$ along the interfaces $\Gamma_i \times (0,T)$, $i = 1,\ldots,N-1$, the DNWR algorithm for the wave equation (1.2) computes for $k = 1,2,\ldots$

$$\begin{aligned} \partial_{tt} u_p^k - c^2(x)\Delta u_p^k &= f, && \text{in } \Omega_p, \\ u_p^k &= g, && \text{on } \partial\Omega \cap \partial\Omega_p, \\ u_p^k &= w_i^{k-1}, && \text{on } \Gamma_i, i = p-1, p, \end{aligned} \tag{2.8}$$

and then for $\ell = 1,2,\ldots,p-1$, it solves in parallel for $i = p-\ell$ and $j = p+\ell$ (continue until $j = N$ for even N)

$$\begin{aligned} \partial_{tt} u_i^k &= c^2(x)\Delta u_i^k + f, \text{ in } \Omega_i, & \partial_{tt} u_j^k &= c^2(x)\Delta u_j^k + f, \text{ in } \Omega_j, \\ u_i^k &= w_{i-1}^{k-1}, \quad \text{on } \Gamma_{i-1}, & \partial_{n_{j,j-1}} u_j^k &= -\partial_{n_{j-1,j}} u_{j-1}^k, \text{ on } \Gamma_{j-1}, \\ \partial_{n_{i,i+1}} u_i^k &= -\partial_{n_{i+1,i}} u_{i+1}^k, \text{ on } \Gamma_i, & u_j^k &= w_j^{k-1}, \quad \text{on } \Gamma_j, \\ u_i^k &= g \quad \text{on } \partial\Omega \cap \partial\Omega_i, & u_j^k &= g, \quad \text{on } \partial\Omega \cap \partial\Omega_j, \end{aligned} \tag{2.9}$$

and the interface data is updated via

$$\begin{aligned} w_i^k(x,t) &= \theta u_i^k\big|_{\Gamma_i \times (0,T)} + (1-\theta) w_i^{k-1}(x,t), \ 1 \le i < p, \\ w_j^k(x,t) &= \theta u_{j+1}^k\big|_{\Gamma_j \times (0,T)} + (1-\theta) w_j^{k-1}(x,t), \ p < j \le N-1, \end{aligned} \tag{2.10}$$

where $\theta \in (0,1]$. Again, a pipeline approach can be used to increase the number of subdomain solves that can be performed in parallel to obtain further speedup.

2.4 DNWR Convergence Estimate for the Wave Equation

We now present our convergence estimate of the DNWR algorithm (2.8)-(2.9)-(2.10) for the specific case of the 1D wave equation with a constant wave speed, $c(x) = c$. As in the heat equation case in 1D, the domain $\Omega := (0,L)$ is decomposed into the subdomains $\Omega_i := (x_{i-1}, x_i)$, $i = 1,\ldots,N$, with subdomain length $h_i := x_i - x_{i-1}$, and since we study the error equations, all the data are zero. We take $\{w_i^0(t)\}_{i=1}^{N-1}$ as initial guesses along the interfaces $\{x = x_i\} \times (0,T)$, and set $w_0^k(t) = w_N^k(t) = 0$ for all k. Denoting by $\{z_i^k(t)\}_{i=1}^{N-1}$ for $k = 1,2\ldots$ the Neumann traces along the interfaces, we compute

$$\begin{aligned} \partial_{tt} u_p^k - c^2 \partial_{xx} u_p^k &= 0, && x \in \Omega_p, \\ u_p^k(x_{p-1}, t) &= w_{p-1}^{k-1}(t), \\ u_p^k(x_p, t) &= w_p^{k-1}(t), \end{aligned} \tag{2.11}$$

for $p = \lceil N/2 \rceil$ and then for $\ell = 1,2,\ldots,p-1$ we solve in parallel for $i = p-\ell$ and $j = p+\ell$ (continue until $j = N$ for even N)

$$\begin{aligned} \partial_{tt} u_i^k - c^2 \partial_{xx} u_i^k &= 0, && x \in \Omega_i, & \partial_{tt} u_j^k - c^2 \partial_{xx} u_j^k &= 0, && x \in \Omega_j, \\ u_i^k(x_{i-1}, t) &= w_{i-1}^{k-1}(t), & & & -\partial_x u_j^k(x_{j-1}, t) &= z_{j-1}^k(t), \\ \partial_x u_i^k(x_i, t) &= z_i^k(t), & & & u_j^k(x_j, t) &= w_j^{k-1}(t), \end{aligned} \tag{2.12}$$

and finally the interface data is updated with the parameter $\theta \in (0,1]$ via

$$\begin{aligned} w_i^k(t) &= \theta u_i^k(x_i,t) + (1-\theta) w_i^{k-1}(t), \qquad & z_i^k(t) &= \partial_x u_{i+1}^k(x_i,t),\ 1 \le i < p, \\ w_j^k(t) &= \theta u_{j+1}^k(x_j,t) + (1-\theta) w_j^{k-1}(t), & z_j^k(t) &= -\partial_x u_j^k(x_j,t),\ p < j \le N-1. \end{aligned} \tag{2.13}$$

We now state the main convergence result for DNWR for the wave equation. The proof of Theorem 2.2 will be given in Subsection 3.3.

Theorem 2.2 (Convergence of DNWR for the wave equation) *Let $\theta = 1/2$. Then the DNWR algorithm for the arrangement (A3), defined in (2.11)–(2.13) converges in at most $k+1$ iterations for multiple subdomains, if the time window length T satisfies $T/k \le h_{\min}/c$, where c is the wave propagation speed.*

3 Analysis of DNWR

In order to prove our main convergence estimate in Theorem 2.1 for the heat equation and in Theorem 2.2 for the wave equation, we need several technical kernel estimates and related results, which we will present next. The proof of the two theorems will then follow in Subsection 3.2 and 3.3, including a generalization to higher spatial dimensions for the wave equation case in Subsection 3.4.

3.1 Kernel Estimates and Auxiliary Results

We need several results related to the Laplace transform to prove our main convergence estimates. For the remainder of the paper, we assume that all functions are piecewise continuous on $(0,\infty)$ and are of exponential order, so that their Laplace transforms $\mathscr{L}\{u(t)\} := \int_0^\infty e^{-st} u(t)\,dt$ exist whenever $\mathrm{Re}(s)$ is large enough. The convolution of two functions $g, w : (0,\infty) \to \mathbb{R}$ is expressed by

$$(g * w)(t) := \int_0^t g(t-\tau) w(\tau) d\tau.$$

We will use the following results from [20] in proving our main theorems.

Result 1 (Lemma 4.1 in [20]) *Let g and w be two real-valued functions in $(0,\infty)$ with $\hat{w}(s) = \mathscr{L}\{w(t)\}$ the Laplace transform of w. Then for $t \in (0,T)$, we have the following properties:*

1. *If $g(t) \ge 0$ and $w(t) \ge 0$, then $(g*w)(t) \ge 0$.*
2. $\|g*w\|_{L^1(0,T)} \le \|g\|_{L^1(0,T)} \|w\|_{L^1(0,T)}$.
3. $\left|(g*w)(t)\right| \le \|g\|_{L^\infty(0,T)} \int_0^T \left|w(\tau)\right| d\tau$.
4. $\int_0^t w(\tau)d\tau = (H*w)(t) = \mathscr{L}^{-1}\left(\frac{\hat{w}(s)}{s}\right)$, *$H(t)$ being the Heaviside step function.*

Result 2 (Lemma 4.2 in [20]) *Let $w(t)$ be a continuous and L^1-integrable function on $(0,\infty)$ with $w(t) \geq 0$ for all $t \geq 0$, and $\hat{w}(s) = \mathscr{L}\{w(t)\}$ be its Laplace transform. Then, for $\tau > 0$, we have the bound*

$$\int_0^\tau |w(t)|\,dt = \int_0^\tau w(t)\,dt \leq \lim_{s\to 0+} \hat{w}(s).$$

Result 3 (Lemma 4.4 in [20]) *Let $\beta > \alpha \geq 0$ and s be a complex variable. Then, for $t \in (0,\infty)$*

$$\varphi(t) := \mathscr{L}^{-1}\left\{\frac{\sinh(\alpha\sqrt{s})}{\sinh(\beta\sqrt{s})}\right\} \geq 0 \quad \textit{and} \quad \psi(t) := \mathscr{L}^{-1}\left\{\frac{\cosh(\alpha\sqrt{s})}{\cosh(\beta\sqrt{s})}\right\} \geq 0.$$

Lemma 3.1 *Let $\alpha, \beta > 0$ be two real numbers and s be a complex variable. Set*

$$\chi(s) := \frac{\sinh((\alpha-\beta)\sqrt{s})}{\cosh(\alpha\sqrt{s})\sinh(\beta\sqrt{s})}. \tag{3.1}$$

Then

$$\int_0^T \left|\mathscr{L}^{-1}\{\chi(\cdot)\}(\tau)\right| d\tau \leq \lim_{s\to 0+} \chi(s) = \left|\frac{\alpha-\beta}{\beta}\right|.$$

Proof There are two possibilities: $\alpha > \beta$ or $\alpha < \beta$. In either case, we need Result 3 to prove non-negativity of the expression, followed by Result 2 to complete the proof. For the full argument, see the proof of Theorem 2 in [37].

The next result establishes useful upper bounds for the inverse Laplace transforms of a few functions that will appear repeatedly in our analysis.

Lemma 3.2 *Suppose $\alpha_1, \alpha_2, \ldots, \alpha_n$ are positive real numbers, with $\alpha = \min_i \alpha_i$. Let $M_i(t)$ be functions defined by their Laplace transforms $\hat{M}_i(s) = \mathscr{L}(M_i(t))$ via*

$$\textit{(i)}\ \hat{M}_1(s) = \frac{\cosh(\alpha\sqrt{s})\cosh((\alpha_1-\alpha_2)\sqrt{s})}{\cosh(\alpha_1\sqrt{s})\cosh(\alpha_2\sqrt{s})},$$

$$\textit{(ii)}\ \hat{M}_2(s) = \frac{\cosh(\alpha\sqrt{s})\sinh(\alpha_1\sqrt{s})\sinh(\alpha_n\sqrt{s})}{\cosh(\alpha_1\sqrt{s})\cosh(\alpha_2\sqrt{s})\cdots\cosh(\alpha_n\sqrt{s})},$$

$$\textit{(iii)}\ \hat{M}_3(s) = \frac{\cosh(\alpha\sqrt{s})\sinh(\alpha_1\sqrt{s})\cosh(\alpha_n\sqrt{s})}{\cosh(\alpha_1\sqrt{s})\cdots\cosh(\alpha_{n-1}\sqrt{s})\sinh(\alpha_n\sqrt{s})},$$

$$\textit{(iv)}\ \hat{M}_4(s) = \frac{\cosh(\alpha\sqrt{s})\sinh(\alpha_1\sqrt{s})}{\cosh(\alpha_1\sqrt{s})\cdots\cosh(\alpha_{n-1}\sqrt{s})\sinh(\alpha_n\sqrt{s})}.$$

Then for any function $u \in L^\infty(0,T)$ with Laplace transform $\hat{u}(s) = \mathscr{L}\{u(t)\}$, we have the following bounds:

$$\textit{(i)}\ \|\mathscr{L}^{-1}\left(\hat{M}_1(s)\,\hat{u}(s)\right)\|_{L^\infty(0,T)} \leq \|u\|_{L^\infty(0,T)}.$$

$$\textit{(ii)}\ \|\mathscr{L}^{-1}\left(\hat{M}_2(s)\,\hat{u}(s)\right)\|_{L^\infty(0,T)} \leq 2\|u\|_{L^\infty(0,T)}.$$

$$\textit{(iii)}\ \|\mathscr{L}^{-1}\left(\hat{M}_3(s)\,\hat{u}(s)\right)\|_{L^\infty(0,T)} \leq \left(\left|\tfrac{\alpha_1-\alpha_n}{\alpha_n}\right| + 1\right)\|u\|_{L^\infty(0,T)}.$$

$$\textit{(iv)}\ \|\mathscr{L}^{-1}\left(\hat{M}_4(s)\,\hat{u}(s)\right)\|_{L^\infty(0,T)} \leq \tfrac{\alpha_1}{\alpha_n}\|u\|_{L^\infty(0,T)}.$$

Proof (i) Using Results 3 and 2, we obtain

$$\int_0^\infty M_1(t)\,dt \le \lim_{s\to 0+} \frac{\cosh(\alpha\sqrt{s})\cosh\left((\alpha_1-\alpha_2)\sqrt{s}\right)}{\cosh(\alpha_2\sqrt{s})\cosh(\alpha_1\sqrt{s})} = 1,$$

so that using Result 1, part 3, we get

$$\left\|\mathscr{L}^{-1}\left(\hat{M}_1(s)\hat{u}(s)\right)\right\|_{L^\infty(0,T)} \le \|u\|_{L^\infty(0,T)}.$$

(ii) We rewrite

$$\begin{aligned}\hat{M}_2(s) &= \frac{-\cosh(\alpha\sqrt{s})}{\cosh(\alpha_2\sqrt{s})\cdots\cosh(\alpha_{n-1}\sqrt{s})}\left(1-\frac{\sinh(\alpha_1\sqrt{s})\sinh(\alpha_n\sqrt{s})}{\cosh(\alpha_1\sqrt{s})\cosh(\alpha_n\sqrt{s})}-1\right)\\ &= -\frac{\cosh(\alpha\sqrt{s})\cosh\left((\alpha_1-\alpha_n)\sqrt{s}\right)}{\cosh(\alpha_1\sqrt{s})\cdots\cosh(\alpha_n\sqrt{s})}+\frac{\cosh(\alpha\sqrt{s})}{\cosh(\alpha_2\sqrt{s})\cdots\cosh(\alpha_{n-1}\sqrt{s})}.\end{aligned}$$

Now since $-\alpha_n \le \alpha_1-\alpha_n \le \alpha_1$, we see that $|\alpha_1-\alpha_n| \le \max\{\alpha_1,\alpha_n\}$. Thus, to obtain a pairing consistent with Result 3, we choose for the case $\alpha_1 \ge \alpha_n$ the pairing

$$\frac{1}{\cosh(\alpha_2\sqrt{s})\cdots\cosh(\alpha_{n-1}\sqrt{s})}\cdot\frac{\cosh\left((\alpha_1-\alpha_n)\sqrt{s}\right)}{\cosh(\alpha_1\sqrt{s})}\cdot\frac{\cosh(\alpha\sqrt{s})}{\cosh(\alpha_n\sqrt{s})}.$$

In the case of $\alpha_1<\alpha_n$, we swap $\cosh(\alpha_1\sqrt{s})$ and $\cosh(\alpha_n\sqrt{s})$ in the denominator. In so doing, we see that the above function corresponds to the convolution of three positive functions, so by Results 3 and 2, we get

$$\begin{aligned}\int_0^\infty |M_2(t)|\,dt &\le \lim_{s\to 0+}\left(\frac{\cosh\left((\alpha_1-\alpha_n)\sqrt{s}\right)\cosh(\alpha\sqrt{s})}{\cosh(\alpha_1\sqrt{s})\cdots\cosh(\alpha_n\sqrt{s})}+\frac{\cosh(\alpha\sqrt{s})}{\cosh(\alpha_2\sqrt{s})\cdots\cosh(\alpha_{n-1}\sqrt{s})}\right)\\ &\le 2,\end{aligned}$$

so that Result 1, part 3 gives

$$\left\|\mathscr{L}^{-1}\left(\hat{M}_2(s)\hat{u}(s)\right)\right\|_{L^\infty(0,T)} \le 2\|u\|_{L^\infty(0,T)}.$$

(iii) We rewrite

$$\begin{aligned}\hat{M}_3(s) &= \frac{\cosh(\alpha\sqrt{s})}{\cosh(\alpha_2\sqrt{s})\cdots\cosh(\alpha_{n-1}\sqrt{s})}\left(\frac{\sinh(\alpha_1\sqrt{s})\cosh(\alpha_n\sqrt{s})}{\cosh(\alpha_1\sqrt{s})\sinh(\alpha_n\sqrt{s})}-1+1\right)\\ &= \frac{\cosh(\alpha\sqrt{s})}{\cosh(\alpha_2\sqrt{s})\cdots\cosh(\alpha_{n-1}\sqrt{s})}\cdot(D_1(s)+1),\end{aligned}$$

where $D_1(s)=\frac{\sinh((\alpha_1-\alpha_n)\sqrt{s})}{\cosh(\alpha_1\sqrt{s})\sinh(\alpha_n\sqrt{s})}$. Now $D_1(s)$ is of the form (3.1). So by Lemma 3.1, we obtain the bound

$$\int_0^\infty |M_3(t)|\,dt \le \lim_{s\to 0+}\frac{\cosh(\alpha\sqrt{s})}{\cosh(\alpha_2\sqrt{s})\cdots\cosh(\alpha_{n-1}\sqrt{s})}(D_1(s)+1) \le \left|\frac{\alpha_1-\alpha_n}{\alpha_n}\right|+1.$$

Finally part 3 of Result 1 proves the inequality.

(iv) We rewrite

$$\begin{aligned}\hat{M}_4(s) &= \frac{\sinh(\alpha\sqrt{s})}{\sinh(\alpha_n\sqrt{s})}\cdot\frac{1}{\cosh(\alpha_2\sqrt{s})\cdots\cosh(\alpha_{n-1}\sqrt{s})}\left(\frac{\sinh(\alpha_1\sqrt{s})\cosh(\alpha\sqrt{s})}{\cosh(\alpha_1\sqrt{s})\sinh(\alpha\sqrt{s})}-1+1\right)\\ &= \frac{\sinh(\alpha\sqrt{s})}{\sinh(\alpha_n\sqrt{s})}\cdot\frac{1}{\cosh(\alpha_2\sqrt{s})\cdots\cosh(\alpha_{n-1}\sqrt{s})}(D_2(s)+1),\end{aligned}$$

where $D_2(s)=\frac{\sinh((\alpha_1-\alpha)\sqrt{s})}{\sinh(\alpha\sqrt{s})\cosh(\alpha_1\sqrt{s})}$. $D_2(s)$ is also of the form (3.1). So by Lemma 3.1, we obtain the bound

$$\begin{aligned}\int_0^\infty |M_4(t)|dt &\le \lim_{s\to 0+}\frac{\sinh(\alpha\sqrt{s})}{\sinh(\alpha_n\sqrt{s})}\cdot\frac{1}{\cosh(\alpha_2\sqrt{s})\cdots\cosh(\alpha_{n-1}\sqrt{s})}(D_2(s)+1)\\ &\le \frac{\alpha}{\alpha_n}\left(\frac{\alpha_1-\alpha}{\alpha}+1\right)=\frac{\alpha_1}{\alpha_n}.\end{aligned}$$

This completes the result.

The following lemma is based on an argument in the proof of Part (ii) of Theorem 2.2 in [20], which we extract and state here separately for completeness.

Lemma 3.3 *Suppose* $f_k(t):=\mathscr{L}^{-1}\left\{\frac{1}{\cosh^k(\alpha\sqrt{s})}\right\}$ *for* $k=1,2,\ldots$. *Then*

(i) $f_k(t)\ge 0$ *for all* t.
(ii) we have the estimate

$$\int_0^T f_k(\tau)\,d\tau \le 2^k\,\mathrm{erfc}\left(\frac{k\alpha}{2\sqrt{T}}\right). \tag{3.2}$$

Proof (i) By Result 3, $f_k(t)\ge 0$ for all t.

(ii) We introduce a non-negative function $r_k(t)$ such that (a) $r_k(t)\ge f_k(t)$ for all t, and (b) its antiderivative is known. This allows us to bound $\int_0^T f_k(\tau)\,d\tau$ by the antiderivative of r_k evaluated at T.
Let $r_k(t):=\mathscr{L}^{-1}(2^k e^{-k\alpha\sqrt{s}})$, which is by [46]

$$\mathscr{L}^{-1}\left(2^k e^{-k\alpha\sqrt{s}}\right)=\frac{2^k\alpha k}{\sqrt{4\pi t^3}}e^{-k^2\alpha^2/4t}. \tag{3.3}$$

Clearly $r_k(t)\ge 0$ for all t. Now we consider

$$\begin{aligned}\mathscr{L}\{r_k(t)-f_k(t)\} &= 2^k e^{-k\alpha\sqrt{s}}-\frac{2^k}{(e^{\alpha\sqrt{s}}+e^{-\alpha\sqrt{s}})^k}\\ &= \frac{2^k((1+e^{-2\alpha\sqrt{s}})^k-1)}{(e^{\alpha\sqrt{s}}+e^{-\alpha\sqrt{s}})^k}=\sum_{j=1}^k\binom{k}{j}e^{-2j\alpha\sqrt{s}}\hat{f}_k(s).\end{aligned}$$

Each term in the sum above corresponds to the convolution of two non-negative functions, which is non-negative. Thus, $r_k(t)-f_k(t)\ge 0$, so we deduce that

$$\int_0^T f_k(\tau)\,d\tau\le\int_0^T r_k(\tau)\,d\tau=\mathscr{L}^{-1}\left(\frac{2^k e^{-k\alpha\sqrt{s}}}{s}\right)=2^k\,\mathrm{erfc}\left(\frac{k\alpha}{2\sqrt{T}}\right),$$

where we expressed the second integral as an inverse Laplace transform using Result 1, part 4, which we then evaluated using the following identity from [46]:

$$\mathscr{L}^{-1}\left(\frac{1}{s}e^{-\lambda\sqrt{s}}\right)=\operatorname{erfc}\left(\frac{\lambda}{2\sqrt{t}}\right),\quad \lambda>0.$$

We have now all the results needed to prove our main convergence estimates announced for the heat equation in Theorem 2.1 and for the wave equation in Theorem 2.2.

3.2 Proof of Theorem 2.1

For clarity of presentation, we show the proof for an odd number of subdomains, $N=2m+1$ and $p=m+1$. The general case is just an extension of the odd case. The outline of the proof is as follows:

- *Part 1:* Derive a recurrence relation for the interface errors in Laplace space: we rewrite the error along the interfaces at iteration k in terms of errors at iteration $k-1$. We will express these errors in terms of their Laplace transforms, since this leads to simpler expressions.
- *Part 2:* Bound each error term in the recurrence relation found in Part 1 using the auxiliary results and lemmas of Section 3.1. Note that one cannot directly estimate the size of a time domain function by bounding its Laplace transform, which is why we rely on the auxiliary results stated in the previous sections.

Part 1: Derivation of recurrence relations. We apply the Laplace transform to the homogeneous Dirichlet subproblem in (2.5), and obtain, using that the initial condition for the error equations is zero,

$$s\hat{u}^k_{m+1}-\nu\partial_{xx}\hat{u}^k_{m+1}=0,\quad \hat{u}^k_{m+1}(x_m,s)=\hat{w}^{k-1}_m(s),\quad \hat{u}^k_{m+1}(x_{m+1},s)=\hat{w}^{k-1}_{m+1}(s).$$

Defining $\sigma_i:=\sinh\left(h_i\sqrt{s/\nu}\right)$ and $\gamma_i:=\cosh\left(h_i\sqrt{s/\nu}\right)$, the solution of the subproblem (2.5) becomes

$$\hat{u}^k_{m+1}(x,s)=\frac{1}{\sigma_{m+1}}\left(\hat{w}^{k-1}_{m+1}(s)\sinh\left((x-x_m)\sqrt{s/\nu}\right)+\hat{w}^{k-1}_m(s)\sinh\left((x_{m+1}-x)\sqrt{s/\nu}\right)\right).$$

Similarly, the solutions of the subproblems (2.6) in Laplace space are

$$\hat{u}^k_i(x,s)=\frac{1}{\gamma_i}\frac{\hat{z}^k_i}{\sqrt{s/\nu}}\sinh((x-x_{i-1})\sqrt{s/\nu})+\frac{1}{\gamma_i}\hat{w}^{k-1}_{i-1}\cosh((x_i-x)\sqrt{s/\nu}),\qquad 1\le i\le m,$$

$$\hat{u}^k_j(x,s)=\frac{1}{\gamma_j}\hat{w}^{k-1}_j\cosh((x-x_{j-1})\sqrt{s/\nu})+\frac{1}{\gamma_j}\frac{\hat{z}^k_{j-1}}{\sqrt{s/\nu}}\sinh((x_j-x)\sqrt{s/\nu}),\qquad m+2\le j\le 2m+1.$$

Therefore, for $\theta=1/2$, we substitute $x=x_i$ or $x=x_j$ into the update conditions (2.7) to obtain the following recurrences for $\hat{w}_i$ and $\hat{w}_j$: for $i=1,\dots,m$ and for $j=m+1,\dots,2m$, we have

$$\hat{w}^k_i=\tfrac{1}{2\gamma_i}\hat{w}^{k-1}_{i-1}+\tfrac{1}{2}\hat{w}^{k-1}_i+\tfrac{\sigma_i}{2\gamma_i}\tfrac{\hat{z}^k_i}{\sqrt{s/\nu}},\qquad \hat{w}^k_j=\tfrac{\sigma_{j+1}}{2\gamma_{j+1}}\tfrac{\hat{z}^k_j}{\sqrt{s/\nu}}+\tfrac{1}{2}\hat{w}^{k-1}_j+\tfrac{1}{2\gamma_{j+1}}\hat{w}^{k-1}_{j+1},\tag{3.4}$$

and for $i = 1,\ldots,m-1$, $j = m+2,\ldots,2m$, we have

$$\hat{z}_i^k = -\sqrt{\tfrac{s}{\nu}}\tfrac{\sigma_{i+1}}{\gamma_{i+1}}\hat{w}_i^{k-1} + \tfrac{1}{\gamma_{i+1}}\hat{z}_{i+1}^k, \qquad \hat{z}_j^k = \tfrac{1}{\gamma_j}\hat{z}_{j-1}^k - \sqrt{\tfrac{s}{\nu}}\tfrac{\sigma_j}{\gamma_j}\hat{w}_j^{k-1}. \tag{3.5}$$

The expressions for $\hat{z}_m$ and $\hat{z}_{m+1}$ are special and are given by

$$\hat{z}_m^k = -\sqrt{\tfrac{s}{\nu}}\tfrac{\gamma_{m+1}}{\sigma_{m+1}}\hat{w}_m^{k-1} + \tfrac{\sqrt{s/\nu}}{\sigma_{m+1}}\hat{w}_{m+1}^{k-1}, \qquad \hat{z}_{m+1}^k = \tfrac{\sqrt{s/\nu}}{\sigma_{m+1}}\hat{w}_m^{k-1} - \sqrt{\tfrac{s}{\nu}}\tfrac{\gamma_{m+1}}{\sigma_{m+1}}\hat{w}_{m+1}^{k-1}.$$

Now for $1 \le i \le m$ and $m+1 \le j \le 2m$, we do a change of variables,

$$\bar{w}_i^k := \gamma_i\hat{w}_i^k, \quad \bar{z}_i^k := \frac{\hat{z}_i^k}{\sqrt{s/\nu}}\sigma_i, \qquad \bar{w}_j^k := \gamma_{j+1}\hat{w}_j^k, \quad \bar{z}_j^k := \frac{\hat{z}_j^k}{\sqrt{s/\nu}}\sigma_{j+1} \tag{3.6}$$

with $\gamma_0 = \gamma_{2m+2} = 1$ in (3.4)–(3.5) to obtain

$$\bar{w}_i^k = \tfrac{1}{2\gamma_{i-1}}\bar{w}_{i-1}^{k-1} + \tfrac{1}{2}\bar{w}_i^{k-1} + \tfrac{1}{2}\bar{z}_i^k, \qquad \bar{w}_j^k = \tfrac{1}{2}\bar{z}_j^k + \tfrac{1}{2}\bar{w}_j^{k-1} + \tfrac{1}{2\gamma_{j+2}}\bar{w}_{j+1}^{k-1},$$

and for $1 \le i \le m-1$ and $m+2 \le j \le 2m$,

$$\bar{z}_i^k = -\tfrac{\sigma_i\sigma_{i+1}}{\gamma_i\gamma_{i+1}}\bar{w}_i^{k-1} + \tfrac{\sigma_i}{\sigma_{i+1}\gamma_{i+1}}\bar{z}_{i+1}^k; \qquad \bar{z}_j^k = \tfrac{\sigma_{j+1}}{\gamma_j\sigma_j}\bar{z}_{j-1}^k - \tfrac{\sigma_j\sigma_{j+1}}{\gamma_j\gamma_{j+1}}\bar{w}_j^{k-1}.$$

The expressions for $\bar{z}_m$ and $\bar{z}_{m+1}$ are again special and are given by

$$\bar{z}_m^k = -\tfrac{\sigma_m\gamma_{m+1}}{\gamma_m\sigma_{m+1}}\bar{w}_m^{k-1} + \tfrac{\sigma_m}{\sigma_{m+1}\gamma_{m+2}}\bar{w}_{m+1}^{k-1}, \qquad \bar{z}_{m+1}^k = \tfrac{\sigma_{m+2}}{\gamma_m\sigma_{m+1}}\bar{w}_m^{k-1} - \tfrac{\gamma_{m+1}\sigma_{m+2}}{\sigma_{m+1}\gamma_{m+2}}\bar{w}_{m+1}^{k-1}.$$

The above recurrences can be summarized as follows. We define the m-vectors $\bar{\mathbf{w}}_L^k$, $\bar{\mathbf{w}}_R^k$, $\bar{\mathbf{z}}_L^k$ and $\bar{\mathbf{z}}_R^k$ such that their components are given by the interface Dirichlet and Neumann traces in Laplace space to the left and to the right of the middle domain:

$$(\bar{\mathbf{w}}_L^k)_i = \bar{w}_i^k, \quad (\bar{\mathbf{w}}_R^k)_i = \bar{w}_{m+i}^k, \quad (\bar{\mathbf{z}}_L^k)_i = \bar{z}_i^k, \quad (\bar{\mathbf{z}}_R^k)_i = \bar{z}_{i+m}^k.$$

Then we see that the recurrences can be rewritten as

$$\bar{\mathbf{w}}_L^k = \frac{1}{2}(T_L\bar{\mathbf{w}}_L^{k-1} + \bar{\mathbf{z}}_L^k), \qquad \bar{\mathbf{w}}_R^k = \frac{1}{2}(T_R\bar{\mathbf{w}}_R^{k-1} + \bar{\mathbf{z}}_R^k), \tag{3.7}$$

$$U_L\bar{\mathbf{z}}_L^k = D_L\bar{\mathbf{w}}_L^{k-1} + E_L\bar{\mathbf{w}}_R^{k-1}, \qquad U_R\bar{\mathbf{z}}_R^k = D_R\bar{\mathbf{w}}_R^{k-1} + E_R\bar{\mathbf{w}}_L^{k-1}, \tag{3.8}$$

where

$$T_L = \begin{bmatrix} 1 & & & \\ \gamma_1^{-1} & 1 & & \\ & \ddots & \ddots & \\ & & \gamma_{m-1}^{-1} & 1 \end{bmatrix}, \qquad T_R = \begin{bmatrix} 1 & \gamma_{m+3}^{-1} & & \\ & \ddots & \ddots & \\ & & \ddots & \gamma_{2m+1}^{-1} \\ & & & 1 \end{bmatrix},$$

$$U_L = \begin{bmatrix} 1 & -\frac{\sigma_1}{\sigma_2\gamma_2} & & \\ & \ddots & \ddots & \\ & & \ddots & -\frac{\sigma_{m-1}}{\sigma_m\gamma_m} \\ & & & 1 \end{bmatrix}, \qquad U_R = \begin{bmatrix} 1 & & & \\ -\frac{\sigma_{m+3}}{\sigma_{m+2}\gamma_{m+2}} & 1 & & \\ & \ddots & \ddots & \\ & & -\frac{\sigma_{2m+1}}{\sigma_{2m}\gamma_{2m}} & 1 \end{bmatrix},$$

$$D_L = \operatorname{diag}\left(-\frac{\sigma_1\sigma_2}{\gamma_1\gamma_2},\dots,-\frac{\sigma_{m-1}\sigma_m}{\gamma_{m-1}\gamma_m},-\frac{\sigma_m\gamma_{m+1}}{\gamma_m\sigma_{m+1}}\right),$$
$$D_R = \operatorname{diag}\left(-\frac{\gamma_{m+1}\sigma_{m+2}}{\sigma_{m+1}\gamma_{m+2}},-\frac{\sigma_{m+2}\sigma_{m+3}}{\gamma_{m+2}\gamma_{m+3}},\dots,-\frac{\sigma_{2m}\sigma_{2m+1}}{\gamma_{2m}\gamma_{2m+1}}\right),$$

and E_L, E_R are matrices that are all zeros except for a single non-zero entry, namely

$$(E_L)_{m,1} = \frac{\sigma_m}{\sigma_{m+1}\gamma_{m+2}}, \qquad (E_R)_{1,m} = \frac{\sigma_{m+2}}{\sigma_{m+1}\gamma_m}.$$

Using (3.8), we can isolate $\bar{\mathbf{z}}_L^k$ and $\bar{\mathbf{z}}_R^k$ and substitute into (3.7) to obtain

$$\bar{\mathbf{w}}_L^k = \frac{1}{2}(T_L + U_L^{-1}D_L)\bar{\mathbf{w}}_L^{k-1} + \frac{1}{2}U_L^{-1}E_L\bar{\mathbf{w}}_R^{k-1},$$
$$\bar{\mathbf{w}}_R^k = \frac{1}{2}(T_R + U_R^{-1}D_R)\bar{\mathbf{w}}_R^{k-1} + \frac{1}{2}U_R^{-1}E_R\bar{\mathbf{w}}_L^{k-1}.$$

The matrices U_L and U_R are easily inverted, and the entries can be explicitly computed as

$$(U_L^{-1})_{i,j} = \begin{cases} 1, & i=j, \\ \frac{\sigma_i}{\sigma_j\gamma_{i+1}\cdots\gamma_j}, & i<j, \\ 0, & \text{otherwise;} \end{cases} \qquad (U_R^{-1})_{i,j} = \begin{cases} 1, & i=j, \\ \frac{\sigma_{m+j}}{\sigma_{m+i}\gamma_{m+j+1}\cdots\gamma_{m+i}}, & i>j, \\ 0, & \text{otherwise.} \end{cases}$$

We can now undo the change of variables in (3.6) to obtain recurrences in terms of $\hat{w}_i^k$. In preparation for the bounds in step 2, we consider rescaling $\hat{w}_i^k$ by defining

$$\hat{v}_i^k = 2^k\gamma^k\hat{w}_i^k, \qquad 1 \le i \le 2m,$$

where $\gamma = \cosh(h\sqrt{s/\nu})$, with $h = \min_i h_i$. Then after some algebra, we obtain

$$\hat{v}_i^k = \sum_{j=1}^{2m} \hat{d}_{i,j}\hat{v}_j^{k-1}, \tag{3.9}$$

where for $1 \le i \le m$, the $\hat{d}_{i,j}$ are given by

$$\hat{d}_{i,j} = \begin{cases} \gamma\left(1-\frac{\sigma_i\sigma_{i+1}}{\gamma_i\gamma_{i+1}}\right), & j=i,\ i<m, \\ \gamma\left(1-\frac{\sigma_m\gamma_{m+1}}{\gamma_m\sigma_{m+1}}\right), & j=i=m, \\ \gamma/\gamma_i, & j=i-1,\ j>1, \\ \frac{-\gamma\sigma_i\sigma_{j+1}}{\gamma_i\gamma_{i+1}\cdots\gamma_{j+1}}, & i+1 \le j \le m-1, \\ \frac{-\gamma\gamma_{m+1}\sigma_i}{\sigma_{m+1}\gamma_i\gamma_{i+1}\cdots\gamma_m}, & j=m,\ i<m, \\ \frac{\gamma\sigma_i}{\sigma_{m+1}\gamma_i\gamma_{i+1}\cdots\gamma_m}, & j=m+1, \\ 0, & \text{otherwise.} \end{cases} \tag{3.10}$$

Noting the similarity between T_L and T_R, D_L and D_R, etc., analogous expressions can be derived for $m+1 \le i \le 2m$ by replacing all indices ℓ in (3.10) by $2m+2-\ell$. We omit the details in the interest of brevity.

Part 2: Error estimation in the time domain. We now estimate the L^∞ norm of $v_i^k(t) := \mathscr{L}^{-1}\{\hat{v}_i^k\}$ by applying the bounds in Results 1–3 as well as Lemma 3.2. For the diagonal entries in the first two lines of (3.10), we take common denominators and use the identities

$$\cosh(y-z) = \cosh y \cosh z - \sinh y \sinh z, \quad \sinh(y-z) = \sinh y \cosh z - \cosh y \sinh z,$$

to see that we can apply either Lemma 3.2 (i) or Result 3 to obtain

$$\|\mathscr{L}^{-1}\{\hat{d}_{i,i}\hat{v}_i^{k-1}\}\|_{L^\infty(0,T)} \leq \begin{cases} \|v_i^{k-1}\|_{L^\infty(0,T)}, & i < m, \\ \frac{|h_m - h_{m+1}|}{h_{m+1}} \|v_m^{k-1}\|_{L^\infty(0,T)}, & i = m. \end{cases}$$

Similarly, the next four lines contain kernels that can be estimated using Result 3 and Lemma 3.2 (ii), (iii) and (iv) respectively. Using the triangle inequality on (3.10) and applying these bounds to each term individually, we obtain

$$\begin{aligned} \|v_i^k(\cdot)\|_{L^\infty(0,T)} &\leq \left(2m - 1 + \frac{2h_{\max}}{h_{m+1}}\right) \max_{1\leq j\leq 2m} \| v_j^{k-1}(\cdot) \|_{L^\infty(0,T)} \\ &\leq \cdots \leq \left(2m - 1 + \frac{2h_{\max}}{h_{m+1}}\right)^k \max_{1\leq j\leq 2m} \| w_j^0(\cdot) \|_{L^\infty(0,T)} . \end{aligned} \tag{3.11}$$

To obtain estimates for the Dirichlet interface values $w_i^k(t)$ themselves, we use the fact that $\mathscr{L}^{-1}\{\gamma^{-k}\} = f_k(t)$ (defined as in Lemma 3.3 with $\alpha = h/\sqrt{\nu}$) to obtain

$$w_i^k(t) = \mathscr{L}^{-1}\{(2\gamma)^{-k} \cdot \hat{v}_i^k(s)\} = \frac{1}{2^k}\left(f_k * v_i^k\right)(t) = \frac{1}{2^k}\int_0^t f_k(t-\tau) v_i^k(\tau) d\tau,$$

from which it follows, using part 3 of Result 1 that

$$\|w_i^k(\cdot)\|_{L^\infty(0,T)} \leq \frac{1}{2^k}\|v_i^k(\cdot)\|_{L^\infty(0,T)} \int_0^T |f_k(\tau)| d\tau. \tag{3.12}$$

Since $\int_0^T |f_k(\tau)|\, d\tau| \leq 2^k \operatorname{erfc}(kh/2\sqrt{\nu T})$ by Lemma 3.3, we combine (3.11) and (3.12) with this bound to conclude the proof of Theorem 2.1.

3.3 Proof of Theorem 2.2

Again we prove this result for odd $N = 2m+1$ only, the proof for even N is analogous. We use a two-part argument similar to Section 3.2:

- *Part 1:* Derive recurrence relations for the error in Laplace space.
- *Part 2:* Use the properties of inverse Laplace transforms to characterize the error and prove convergence of the method in the time domain.

Part 1: Derivation of recurrence relations. We apply the Laplace transform to the homogeneous Dirichlet subproblem in (2.11) to get

$$s^2\hat{u}^k_{m+1} - c^2\partial_{xx}\hat{u}^k_{m+1} = 0, \quad \hat{u}^k_{m+1}(x_m,s) = \hat{w}^{k-1}_m(s), \quad \hat{u}^k_{m+1}(x_{m+1},s) = \hat{w}^{k-1}_{m+1}(s).$$

Define $\rho_i := \sinh(h_i s/c)$ and $\lambda_i := \cosh(h_i s/c)$. Then the solution of subproblem (2.11) becomes

$$\hat{u}^k_{m+1}(x,s) = \frac{1}{\rho_{m+1}}\left(\hat{w}^{k-1}_{m+1}(s)\sinh((x-x_m)s/c) + \hat{w}^{k-1}_m(s)\sinh((x_{m+1}-x)s/c)\right).$$

The solutions of the subproblems (2.12) in Laplace space are

$$\begin{aligned}
\hat{u}^k_i(x,s) &= \tfrac{1}{\lambda_i}\tfrac{\hat{z}^k_i}{s/c}\sinh((x-x_{i-1})s/c) + \tfrac{1}{\lambda_i}\hat{w}^{k-1}_{i-1}\cosh((x_i-x)s/c),\ 1\le i\le m,\\
\hat{u}^k_j(x,s) &= \tfrac{1}{\lambda_j}\hat{w}^{k-1}_j\cosh((x-x_{j-1})s/c) + \tfrac{1}{\lambda_j}\tfrac{\hat{z}^k_{j-1}}{s/c}\sinh((x_j-x)s/c),\ m+2\le j\le 2m+1.
\end{aligned}$$

Therefore for $\theta = 1/2$ the update conditions (2.13) become

$$\begin{aligned}
\hat{w}^k_i &= \tfrac{1}{2\lambda_i}\hat{w}^{k-1}_{i-1} + \tfrac{1}{2}\hat{w}^{k-1}_i + \tfrac{\rho_i}{2\lambda_i}\tfrac{\hat{z}^k_i}{s/c},\ 1\le i\le m,\\
\hat{w}^k_j &= \tfrac{\rho_{j+1}}{2\lambda_{j+1}}\tfrac{\hat{z}^k_j}{s/c} + \tfrac{1}{2}\hat{w}^{k-1}_j + \tfrac{1}{2\lambda_{j+1}}\hat{w}^{k-1}_{j+1},\ m+1\le j\le 2m.
\end{aligned} \tag{3.13}$$

and, for $1\le i\le m-1$ and $m+2\le j\le 2m$,

$$\begin{aligned}
\hat{z}^k_i &= -\tfrac{s}{c}\tfrac{\rho_{i+1}}{\lambda_{i+1}}\hat{w}^{k-1}_i + \tfrac{1}{\lambda_{i+1}}\hat{z}^k_{i+1};\ \hat{z}^k_m = -\tfrac{s}{c}\tfrac{\lambda_{m+1}}{\rho_{m+1}}\hat{w}^{k-1}_m + \tfrac{s/c}{\rho_{m+1}}\hat{w}^{k-1}_{m+1},\\
\hat{z}^k_{m+1} &= \tfrac{s/c}{\rho_{m+1}}\hat{w}^{k-1}_m - \tfrac{s}{c}\tfrac{\lambda_{m+1}}{\rho_{m+1}}\hat{w}^{k-1}_{m+1};\quad \hat{z}^k_j = \tfrac{1}{\lambda_j}\hat{z}^k_{j-1} - \tfrac{s}{c}\tfrac{\rho_j}{\lambda_j}\hat{w}^{k-1}_j.
\end{aligned} \tag{3.14}$$

For $1\le i\le m$ and $m+1\le j\le 2m$ we do a change of variables

$$\bar{w}^k_i := \lambda_i\hat{w}^k_i,\ \bar{z}^k_i := \frac{\hat{z}^k_i}{s/c}\rho_i,\ \bar{w}^k_j := \lambda_{j+1}\hat{w}^k_j,\ \bar{z}^k_j := \frac{\hat{z}^k_j}{s/c}\rho_{j+1},$$

with $\lambda_0 = \lambda_{2m+2} = 1$ in the corresponding equations of (3.13)-(3.14) to get

$$\begin{aligned}
w^k_i &= \tfrac{1}{2\lambda_{i-1}}\bar{w}^{k-1}_{i-1} + \tfrac{1}{2}\bar{w}^{k-1}_i + \tfrac{1}{2}\bar{z}^k_i,\ 1\le i\le m;\\
\bar{w}^k_j &= \tfrac{1}{2}\bar{z}^k_j + \tfrac{1}{2}\bar{w}^{k-1}_j + \tfrac{1}{2\lambda_{j+2}}\bar{w}^{k-1}_{j+1},\ m+1\le j\le 2m,
\end{aligned}$$

and, for $1\le i\le m-1$ and $m+2\le j\le 2m$,

$$\begin{aligned}
\bar{z}^k_i &= -\tfrac{\rho_i\rho_{i+1}}{\lambda_i\lambda_{i+1}}\bar{w}^{k-1}_i + \tfrac{\rho_i}{\rho_{i+1}\lambda_{i+1}}\bar{z}^k_{i+1};\ \bar{z}^k_m = -\tfrac{\rho_m\lambda_{m+1}}{\lambda_m\rho_{m+1}}\bar{w}^{k-1}_m + \tfrac{\rho_m}{\rho_{m+1}\lambda_{m+2}}\bar{w}^{k-1}_{m+1},\\
\bar{z}^k_{m+1} &= \tfrac{\rho_{m+2}}{\lambda_m\rho_{m+1}}\bar{w}^{k-1}_m - \tfrac{\lambda_{m+1}\rho_{m+2}}{\rho_{m+1}\lambda_{m+2}}\bar{w}^{k-1}_{m+1};\quad \bar{z}^k_j = \tfrac{\rho_{j+1}}{\lambda_j\rho_j}\bar{z}^k_{j-1} - \tfrac{\rho_j\rho_{j+1}}{\lambda_j\lambda_{j+1}}\bar{w}^{k-1}_j.
\end{aligned}$$

We can now mimic the manipulation in the proof of Theorem 2.1, but with the γ_i and σ_i replaced by λ_i and ρ_i instead. Then the update conditions become

$$\hat{w}^k_i(s) = \sum_{l=i-1}^{m+1}\hat{\beta}_{i,l}\hat{w}^{k-1}_l(s),\ 1\le i\le m;\quad \hat{w}^k_j(s) = \sum_{l=m}^{j+1}\hat{\beta}_{j,l}\hat{w}^{k-1}_l(s),\ m+1\le j\le 2m, \tag{3.15}$$

where the coefficients $\hat{\beta}_{i,j}$ are given by $\hat{\beta}_{1,0} = \hat{\beta}_{2m,2m+1} = 0$, and for $i+1 \leq l < m$, $1 \leq i < m$,

$$\hat{\beta}_{i,i-1} = \frac{1}{2\lambda_i}, \; \hat{\beta}_{i,i} = \frac{\lambda_{i,i+1}}{2\lambda_i\lambda_{i+1}}, \; \hat{\beta}_{i,l} = -\frac{\rho_i\rho_{l+1}}{2\lambda_i\lambda_{i+1}\ldots\lambda_{l+1}},$$
$$\hat{\beta}_{i,m} = -\frac{\rho_i\lambda_{m+1}}{2\lambda_i\ldots\lambda_m\rho_{m+1}}, \; \hat{\beta}_{i,m+1} = \frac{\rho_i}{2\lambda_i\ldots\lambda_m\rho_{m+1}},$$

and for $m+1 < l \leq j-1$, $m+1 < j \leq 2m$

$$\hat{\beta}_{j,j} = \frac{\lambda_{j,j+1}}{2\lambda_j\lambda_{j+1}}, \; \hat{\beta}_{j,l} = -\frac{\rho_{j+1}\rho_l}{2\lambda_l\lambda_{l+1}\ldots\lambda_{j+1}}, \; \hat{\beta}_{j,j+1} = \frac{1}{2\lambda_{j+1}},$$
$$\hat{\beta}_{j,m+1} = -\frac{\rho_{j+1}\lambda_{m+1}}{2\rho_{m+1}\lambda_{m+2}\ldots\lambda_{j+1}}, \; \hat{\beta}_{j,m} = \frac{\rho_{j+1}}{2\rho_{m+1}\lambda_{m+2}\ldots\lambda_{j+1}}.$$

Also,

$$\hat{\beta}_{m,m-1} = \frac{1}{2\lambda_m}, \; \hat{\beta}_{m,m} = \frac{\rho_{m+1,m}}{2\rho_{m+1}\lambda_m}, \; \hat{\beta}_{m,m+1} = \frac{\rho_m}{2\rho_{m+1}\lambda_m},$$
$$\hat{\beta}_{m+1,m} = \frac{\rho_{m+2}}{2\rho_{m+1}\lambda_{m+2}}, \; \hat{\beta}_{m+1,m+1} = \frac{\rho_{m+1,m+2}}{2\rho_{m+1}\lambda_{m+2}}, \; \hat{\beta}_{m+1,m+2} = \frac{1}{2\lambda_{m+2}}.$$

Part 2: Characterization of the error in the time domain. By induction on (3.15) we can write for $1 \leq i \leq 2m$,

$$\hat{w}_i^k(s) = \sum_{j=1}^{2m} \vartheta_{i,j}^n \left(\hat{\beta}_{1,1}, \hat{\beta}_{1,2}, \ldots, \hat{\beta}_{2m,2m-1}, \hat{\beta}_{2m,2m}\right) \hat{w}_j^{k-n}(s), \tag{3.16}$$

where the coefficients $\vartheta_{i,j}^n$ are either zero or homogeneous polynomials of degree n. Next we expand the hyperbolic functions into infinite series of exponential functions using the geometric series expansion, based on the identity

$$\cosh(z) = \frac{1}{2}(e^z + e^{-z}) = \frac{e^z}{2}(1 + e^{-2z}).$$

This allows us to rewrite the coefficients $\hat{\beta}_{i,j}$ as follows: for $i+1 \leq l < m$ and $1 \leq i < m$, we have for the (i,i)th entry

$$\begin{aligned}
\hat{\beta}_{i,i} &= \frac{\cosh\left((h_i - h_{i+1})s/c\right)}{2\cosh(h_i s/c)\cosh(h_{i+1}s/c)} \\
&= \frac{e^{(h_i - h_{i+1})s/c)} + e^{(h_{i+1}-h_i)s/c}}{e^{h_i s/c}(1+e^{-2h_i s/c}) \cdot e^{h_{i+1}s/c}(1+e^{-2h_{i+1}s/c})} \\
&= (e^{-2h_{i+1}s/c} + e^{-2h_i s/c})(1+e^{-2h_i s/c})^{-1}(1+e^{-2h_{i+1}s/c})^{-1} \\
&= \left(e^{-2h_i s/c} + e^{-2h_{i+1}s/c}\right)\left[1 + \sum_{l=1}^{\infty}(-1)^l e^{-2h_i l s/c} + \sum_{n=1}^{\infty}(-1)^n e^{-2h_{i+1}ns/c} + \sum_{l=1}^{\infty}\sum_{n=1}^{\infty}(-1)^{l+n} e^{-2(lh_i + nh_{i+1})s/c}\right].
\end{aligned}$$

Similarly, the other coefficients can be expanded as follows:

$$\begin{aligned}
\hat{\beta}_{i,l} &= -\frac{\sinh(h_i s/c)\sinh(h_{l+1}s/c)}{2\cosh(h_i s/c)\cosh(h_{i+1}s/c)\ldots\cosh(h_{l+1}s/c)} \\
&= -2^{l-i-1}e^{-(h_{i+1}+\cdots+h_l)s/c}\left(1-e^{-2h_i s/c}-e^{-2h_{l+1}s/c}+e^{-2(h_i+h_{l+1})s/c}\right)\prod_{n=i}^{l+1}\left(1+e^{-2h_n s/c}\right)^{-1}, \\
\hat{\beta}_{i,i-1} &= \frac{1}{2\cosh(h_i s/c)} = e^{-h_i s/c}\left[1+\sum_{l=1}^{\infty}(-1)^l e^{-2h_i l s/c}\right], \\
\hat{\beta}_{i,m} &= -\frac{\sinh(h_i s/c)\cosh(h_{m+1}s/c)}{2\cosh(h_i s/c)\ldots\cosh(h_m s/c)\sinh(h_{m+1}s/c)} \\
&= -2^{m-i-1}e^{-(h_{i+1}+\cdots+h_m)s/c}\left(1-e^{-2h_i s/c}+e^{-2h_{m+1}s/c}\ -e^{-2(h_i+h_{m+1})s/c}\right)\left(1-e^{-2h_{m+1}s/c}\right)^{-1}\prod_{l=i}^{m}\left(1+e^{-2h_l s/c}\right)^{-1}, \\
\hat{\beta}_{i,m+1} &= \frac{\sinh(h_i s/c)}{2\cosh(h_i s/c)\ldots\cosh(h_m s/c)\sinh(h_{m+1}s/c)} \\
&= 2^{m-i}e^{-(h_{i+1}+\cdots+h_{m+1})s/c}\left(1-e^{-2h_i s/c}\right)\left(1-e^{-2h_{m+1}s/c}\right)^{-1}\prod_{l=i}^{m}\left(1+e^{-2h_l s/c}\right)^{-1}, \\
\hat{\beta}_{m,m} &= \frac{\sinh((h_{m+1}-h_m)s/c)}{2\cosh(h_m s/c)\sinh(h_{m+1}s/c)} \\
&= \left(e^{-2h_m s/c}-e^{-2h_{m+1}s/c}\right)\left[1+\sum_{l=1}^{\infty}(-1)^l e^{-2h_m l s/c}+\sum_{n=1}^{\infty}e^{-2h_{m+1}ns/c}+\sum_{l=1}^{\infty}\sum_{n=1}^{\infty}(-1)^l e^{-2(lh_m+nh_{m+1})s/c}\right], \\
\hat{\beta}_{m,m+1} &= \frac{\sinh(h_m s/c)}{2\cosh(h_m s/c)\sinh(h_{m+1}s/c)} \\
&= \left(e^{-h_{m+1}s/c}-e^{-(2h_m+h_{m+1})s/c}\right)\left[1+\sum_{l=1}^{\infty}(-1)^l e^{-2h_m l s/c}+\sum_{n=1}^{\infty}e^{-2h_{m+1}ns/c}+\sum_{l=1}^{\infty}\sum_{n=1}^{\infty}(-1)^l e^{-2(lh_m+nh_{m+1})s/c}\right].
\end{aligned}$$

The other terms are expanded similarly using the geometric series. The resulting expressions allow us to rewrite Equation (3.16) as

$$\hat{w}_i^k(s) = \sum_{j=1}^{2m}\hat{r}_{i,j}^k(s)\,\hat{w}_j^0(s), \tag{3.17}$$

with each $\hat{r}_{i,j}^k(s)$ being a linear combination of terms of the form $e^{-s\zeta}$, with $\zeta \geq kh_l/c$ for some $l \in \{1,2,\ldots 2m+1\}$. Using the shifting property of the inverse Laplace transform, i.e.,

$$\mathscr{L}^{-1}\left\{e^{-\zeta s}\hat{f}(s)\right\} = H(t-\zeta)f(t-\zeta) = \begin{cases} f(t-\zeta), & t>\zeta, \\ 0, & t\leq\zeta, \end{cases} \tag{3.18}$$

we conclude that

$$w_i^k(t) = w_j^0\left(t-\frac{kh_l}{c}\right)H\left(t-\frac{kh_l}{c}\right) + \text{other terms} \tag{3.19}$$

for some $j \in \{1,2,\ldots 2m\}$ and $l \in \{1,2,\ldots 2m+1\}$, where all the unlisted terms vanish for $t \leq kh_l/c$. Therefore, for $T \leq kh_{\min}/c$, we get $w_i^k(t) = 0$ for all i, and this completes the proof of Theorem 2.2.

Remark 3.1 It has already been shown in [38] that the shifting property (3.18) plays an important role in proving the finite termination property of NNWR. Here, we observe the same property for DNWR for $\theta = 1/2$: the right hand side of (3.19) becomes identically zero for $t \leq kh_l/c$, so for any finite window length T, the interface error eventually becomes zero everywhere in $[0,T]$ when k is large enough, so the method converges to the exact solution at the next iteration.

3.4 Analysis of the DNWR Algorithm for the Wave Equation in 2D

We now generalize our results to higher spatial dimensions using Fourier transform techniques. As a model problem, we consider the two-dimensional wave equation

$$\partial_{tt}u - c^2\Delta u = f(x,y,t), \quad (x,y) \in \Omega = (l,L)\times(0,\pi),\, t \in (0,T]$$

with initial conditions $u(x,y,0) = u_0(x,y)$, $\partial_t u(x,y,0) = v_0(x,y)$ and Dirichlet boundary conditions $u(x,y,t) = g(x,y,t)$, $(x,y) \in \partial\Omega$. First, our domain of interest Ω is decomposed into strips of the form $\Omega_i = (x_{i-1},x_i)\times(0,\pi)$, $l = x_0 < x_1 < \cdots < x_N = L$. Suppose the subdomain widths are $h_i := x_i - x_{i-1}$, and denote by $h_{\min}$ the minimum among these widths, i.e., $h_{\min} := \min_{1\leq i\leq N} h_i$.

For analysis purposes, we will consider the error equations, which is equivalent to setting all initial and boundary conditions to zero, in addition to considering a zero forcing term. This allows us to write the DNWR algorithm for the error equations as follows: for the initial errors $\{w_i^0(y,t)\}_{i=1}^{N-1}$ along the interfaces $\{x = x_i\}$, the interior error u_p^k on subdomain p is obtained from the the interface errors at iteration $k-1$ for $p = \lceil N/2\rceil$ and $k = 1,2,\ldots$

$$\begin{aligned} \partial_{tt}u_p^k - c^2\Delta u_p^k &= 0, && \text{in } \Omega_p,\\ u_p^k(x_{p-1},y,t) &= w_{p-1}^{k-1}(y,t),\\ u_p^k(x_p,y,t) &= w_p^{k-1}(y,t),\\ u_p^k(x,0,t) &= u_p^k(x,\pi,t) = 0, \end{aligned} \tag{3.20}$$

Next, denoting by $\{z_i^k(y,t)\}_{i=1}^{N-1}$ the Neumann traces along the interfaces, for $\ell = 1,2,\ldots,p-1$ we compute in parallel with $i = p-\ell$ and $j = p+\ell$ (continue until $j = N$ for even N)

$$\begin{aligned} &\partial_{tt}u_i^k - c^2\Delta u_i^k = 0, && \text{in } \Omega_i, \qquad \partial_{tt}u_j^k - c^2\Delta u_j^k = 0, && \text{in } \Omega_j,\\ &u_i^k(x_{i-1},y,t) = w_{i-1}^{k-1}(y,t), && -\partial_x u_j^k(x_{j-1},y,t) = z_{j-1}^k(y,t),\\ &\partial_x u_i^k(x_i,y,t) = z_i^k(y,t), && u_j^k(x_j,y,t) = w_j^{k-1}(y,t),\\ &u_i^k(x,0,t) = u_i^k(x,\pi,t) = 0, && u_j^k(x,0,t) = u_j^k(x,\pi,t) = 0. \end{aligned} \tag{3.21}$$

The update conditions for $1 \leq i < p$ and $p \leq j \leq N-1$ are then given by

$$\begin{aligned} w_i^k(y,t) &= \theta u_i^k(x_i,y,t) + (1-\theta)w_i^{k-1}(y,t), \quad z_i^k(y,t) = \partial_x u_{i+1}^k(x_i,y,t),\\ w_j^k(y,t) &= \theta u_{j+1}^k(x_j,y,t) + (1-\theta)w_j^{k-1}(y,t), \; z_j^k(y,t) = -\partial_x u_j^k(x_j,y,t), \end{aligned} \tag{3.22}$$

where $\theta \in (0,1]$.

We analyze this 2D case by transforming it into a collection of 1D problems using the Fourier sine transform along the y direction. Expanding the solution in a Fourier sine series along the y-direction yields

$$u_i^k(x,y,t) = \sum_{n\geq 1} U_i^k(x,n,t)\sin(ny),$$

where

$$U_i^k(x,n,t) = \frac{2}{\pi}\int_0^\pi u_i^k(x,\eta,t)\sin(n\eta)d\eta.$$

We obtain a sequence of 1D problems corresponding to $n \in \mathbb{N}$ from (3.20),

$$\frac{\partial^2 U_p^k}{\partial t^2}(x,n,t) - c^2\frac{\partial^2 U_p^k}{\partial x^2}(x,n,t) + c^2 n^2 U_p^k(x,n,t) = 0, \tag{3.23}$$

with corresponding boundary conditions for $U_p^k(x,n,t)$. To present the main convergence result we define the function

$$\chi(\alpha,\beta,t) := \mathscr{L}^{-1}\left\{\exp\left(-\beta\sqrt{s^2+\alpha^2}\right)\right\}, \quad \mathrm{Re}(s) > 0, \tag{3.24}$$

with s being the Laplace variable, and we recall a result from [38]:

Result 4 (Lemma 3.1 in [38]) *We have the identity*

$$\chi(\alpha,\beta,t) = \begin{cases} \delta(t-\beta) - \frac{\alpha\beta}{\sqrt{t^2-\beta^2}}J_1\left(\alpha\sqrt{t^2-\beta^2}\right), & t \geq \beta, \\ 0, & 0 < t < \beta, \end{cases}$$

where δ is the Dirac delta function and J_1 is the Bessel function of first order given by

$$J_1(z) = \frac{1}{\pi}\int_0^\pi \cos\left(z\sin\varphi - \varphi\right)d\varphi.$$

We now prove the convergence result of the DNWR method for the 2D wave equation. Even though the algorithm works very differently from the Neumann–Neumann Waveform Relaxation (NNWR) method, the proofs of convergence are very similar, see the proof for NNWR in [38, Theorem 3.2].

Theorem 3.1 (Convergence of DNWR for the wave equation in 2D) *Let $\theta = 1/2$. For $T > 0$ fixed, the DNWR algorithm applied to the arrangement (A3) of the strip decomposition (3.20)–(3.22) converges in at most $k+1$ iterations, if the time window length T satisfies $T/k < h_{\min}/c$, c being the wave speed.*

Proof We prove the theorem only for $N = 2m+1$, since the case for even N is similar. Applying Laplace transforms in the t variable on the equation (3.23), we obtain

$$(s^2 + c^2n^2)\hat{U}_{m+1}^k - c^2\frac{d^2\hat{U}_{m+1}^k}{dx^2} = 0.$$

For each $n = 1,2,\ldots$, this equation is similar to the one-dimensional analysis in the proof of Theorem 2.2, except s^2 is replaced by $s^2 + c^2n^2$. Therefore, the interface solutions $\hat{W}_i^k(n,s)$ satisfy (3.17), but with s replaced by $\sqrt{s^2+c^2n^2}$, i.e., we have

$$\hat{W}_i^k(n,s) = \sum_j \hat{r}_{i,j}^k\left(\sqrt{s^2+c^2n^2}\right)\hat{W}_j^0(n,s). \tag{3.25}$$

The coefficients $\hat{r}_{i,j}^k(s)$ in (3.25) are linear combinations of terms of the form $e^{-\zeta s}$ for $\zeta \geq kh_l/c$ for some $l \in \{1,2,\ldots 2m+1\}$. Thus, the coefficients $\hat{r}_{i,j}^k\left(\sqrt{s^2+c^2n^2}\right)$ are sums of exponential functions of the form $e^{-\zeta\sqrt{s^2+c^2n^2}}$ for $\zeta \geq kh_l/c$. Using the properties of χ in (3.24), we deduce that the inverse Laplace transform of (3.25) satisfies

$$W_i^k(n,t) = \sum_j \sum_l \chi(cn,\zeta_{l,j},t) * W_j^0(n,t),$$

with $\zeta_{l,j} \geq kh_{\min}/c$. Result 4 then implies that for $t < kh_{\min}/c$ and $n = 1,2,\ldots$, $W_i^k(n,t) = 0$. Now the interface errors $w_i^k(y,t)$ are given by

$$w_i^k(y,t) = \sum_{n\geq 1} W_i^k(n,t)\sin(ny),$$

and they become zero for all $i \in \{1,\ldots,2m\}$. Since the errors are zero, the next iteration yields the exact solution in the whole domain.

4 Numerical Experiments

We now show numerical experiments, first for the heat equation, and then also for the wave equation, and situations which are not covered by our analysis, namely problems with non-constant coefficients and non-matching time grids.

4.1 Heat Equation in 1D

We consider the heat equation $\partial_t u = \Delta u$ in $\Omega = (0,5)$, with initial condition $u_0(x) = x(5-x)$ and boundary conditions $u(0,t) = t^2$, $u(5,t) = te^{-t}$, discretized using standard centered finite differences in space and backward Euler in time on a grid with $\Delta x = 2\times 10^{-2}$ and $\Delta t = 4\times 10^{-3}$. In the first experiment we apply DNWR for a decomposition into five subdomains and for three different time window sizes, $T = 0.2, 2, 8$, see Figure 4.1 on the left. In a second experiment we fix the time window size to $T = 2$ and use three to six equal subdomains, see Figure 4.1 on the right. We observe superlinear convergence as predicted by Theorem 2.1, and for small T the estimate is quite sharp. We also see that the convergence slows down as the number of subdomains increases, which is consistent with the classical SWR and NNWR methods [23,20].

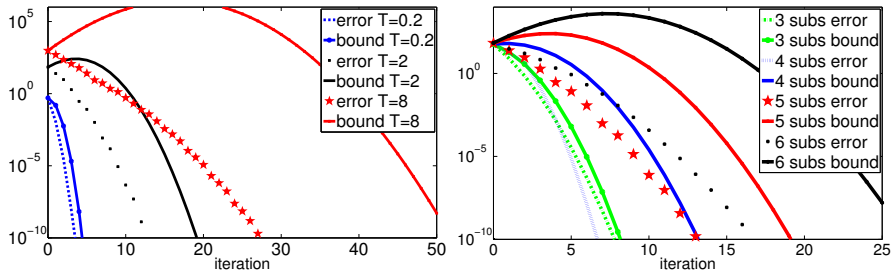

Fig. 4.1: Convergence of DNWR for the 1D heat equation. We show the measured error and our theoretical estimates for $\theta = 1/2$, on the left for various time window length T for five subdomains, and on the right for various number of subdomains for $T = 2$

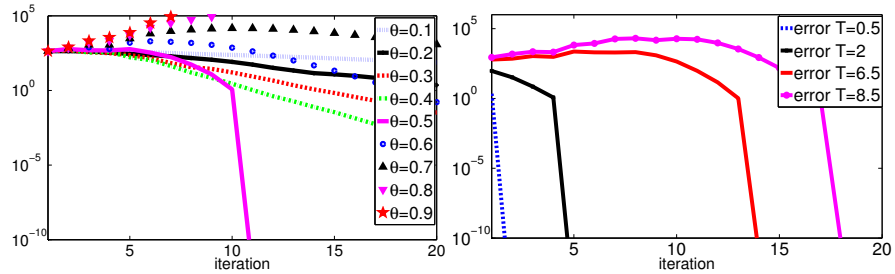

Fig. 4.2: Convergence of DNWR for the 1D wave equation, with various values of θ for $T = 5$ on the left, and for various lengths T of the time window and $\theta = 1/2$ on the right, using the arrangement A3

4.2 Wave Equation in 1D

We now consider the wave equation $\partial_{tt}u = \partial_{xx}u$ in $\Omega = (0,5)$, with zero initial conditions and boundary conditions $u(0,t) = t^2$, $u(5,t) = t^2e^{-t}$, discretized using centered finite differences in both space and time on a grid with $\Delta x = \Delta t = 2\times10^{-2}$. We consider a decomposition of Ω into five unequal subdomains, whose widths h_i are $1, 0.5, 1.5, 1, 1$, so that $h_{\min} = 0.5$, and take as initial guess $w_j^0(t) = t^2$, $t \in (0,T]$ for $1 \le j \le 4$. On the left in Figure 4.2, we show the convergence for different values of the parameter θ for $T = 5$, and on the right the error curves for the best parameter $\theta = 1/2$ for different time window length T. These convergence curves illustrate well our convergence result in Theorem 2.2 obtained for the arrangement A3: we observe convergence in a finite number of steps depending on T for $\theta = 1/2$.

In Figure 4.3 and Figure 4.4, we show the corresponding results for the other arrangements A1 and A2 described in Section 2, and we see that changing the arrangement has an influence on the error in the initial iterations, but not on the finite-step convergence property: indeed, just as predicted in Theorem 2.2 for the arrangement

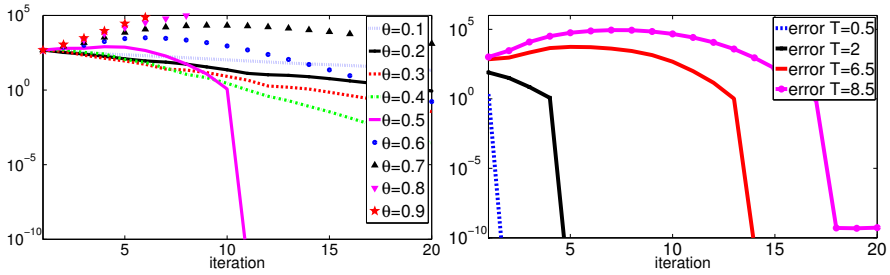

Fig. 4.3: Same experiments as in Figure 4.2, but for arrangement A1

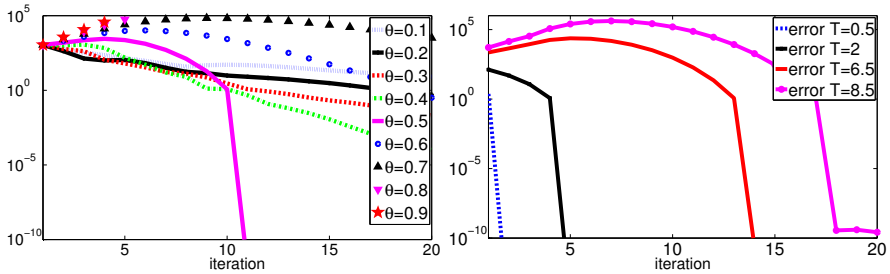

Fig. 4.4: Same experiments as in Figure 4.2, but for arrangement A2.

A3, the error in all three arrangements falls within round-off error after 2, 5, 14 and 18 iterations, which corresponds to $2T+1$ iterations for $T = 0.5, 2, 6.5, 8.5$ respectively.

4.3 Wave Equation in 2D

We next show a numerical experiment for the DNWR algorithm applied to the two dimensional wave equation $\partial_{tt}u-(\partial_{xx}u+\partial_{yy}u)=0$ with initial conditions $u(x,y,0)=xy(x-1)(y-\pi)(5x-2)(4x-3)$, $u_t(x,y,0)=0$, and homogeneous Dirichlet boundary conditions. We discretize the wave equation using centered finite differences in both space and time on a grid with $\Delta x = 5\times10^{-2}$, $\Delta y = 16\times10^{-2}$, and $\Delta t = 4\times10^{-2}$. We decompose our domain $\Omega := (0,1)\times(0,\pi)$ into three non-overlapping subdomains $\Omega_1 = (0,2/5)\times(0,\pi)$, $\Omega_2 = (2/5,3/4)\times(0,\pi)$, $\Omega_3 = (3/4,1)\times(0,\pi)$. As initial guess, we take $w_i^0(y,t) = t\sin(y)$. In Figure 4.5 we plot the convergence curves for different values of the parameter θ for $T=2$ on the left, and on the right the results for the best parameter $\theta = 1/2$ for different time window length T, and we observe again convergence in a finite number of steps for the optimal choice $\theta = 1/2$.

4.4 Comparison of DNWR with NNWR and SWR

We now compare the performance of the DNWR method to the Neumann-Neumann Waveform Relaxation (NNWR) method from [38,21], and the Schwarz Waveform

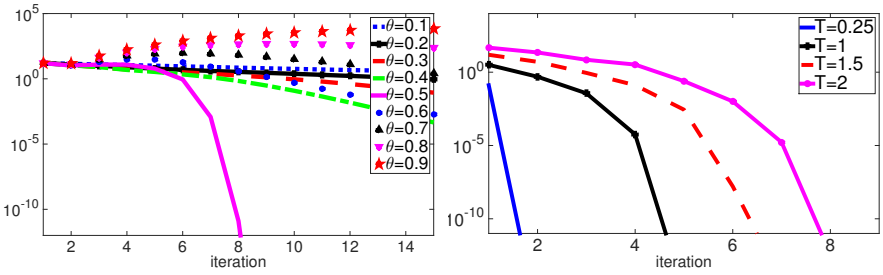

Fig. 4.5: Convergence of DNWR for the wave equation in 2D: curves for different values of θ for $T = 2$ on the left, and for various time window lengths T and $\theta = 1/2$ on the right

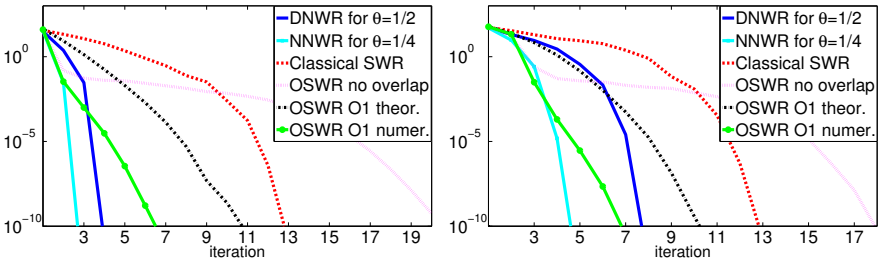

Fig. 4.6: Comparison of DNWR, NNWR, and SWR for $T = 2$ for the 2D wave equation for two subdomains on the left, and three subdomains on the right

Relaxation (SWR) methods with and without overlap from [16,14]. We consider the 2D wave equation $\partial_{tt}u - (\partial_{xx}u + \partial_{yy}u) = 0$ on the domain $\Omega := (0,1) \times (0,\pi)$ with homogeneous initial conditions, and Dirichlet boundary conditions $u(0,y,t) = t^2 \sin(y)$, $u(1,y,t) = y(y-\pi)t^3$ and $u(x,0,t) = 0 = u(x,\pi,t)$. For the two subdomain experiment, we decompose our domain into $\Omega_1 = (0,3/5) \times (0,\pi)$ and $\Omega_2 = (3/5,1) \times (0,\pi)$, and for the three subdomain experiment into $\Omega_1 = (0,2/5) \times (0,\pi)$, $\Omega_2 = (2/5,3/4) \times (0,\pi)$, $\Omega_3 = (3/4,1) \times (0,\pi)$. We take a random initial guess to start the iteration, and for the overlapping SWR we use an overlap of $2\Delta x$ in all the experiments. We used first order transmission conditions with one parameter in the optimized SWR iterations; for more details see [14]. On the left in Figure 4.6, we show the convergence curves for the various methods for two subdomains, and on the right for three subdomains. We see that NNWR is about twice as fast as DNWR, but also needs two subdomain solves per iteration, whereas DNWR only needs one, so these methods are comparable, as indicated by the results from our analysis and the analyses in [38,21], summarized in Table 4.1. From Figure 4.6 we also see that classical SWR is much slower than DNWR ad NNWR, but the optimized variants can be competitive, especially for low iteration numbers where they are the fastest.

Table 4.1: Comparison of iteration steps k needed for convergence of DNWR and NNWR for the wave equation.

Methods	2 subdomains, 1D	Many subdomains, 1D	Many subdomains, 2D
DNWR	$T \leq 2kh_{\min}/c$	$T \leq kh_{\min}/c$	$T < kh_{\min}/c$
NNWR	$T \leq 4kh_{\min}/c$	$T \leq 2kh_{\min}/c$	$T < 2kh_{\min}/c$

Table 4.2: Wave speed and time steps for different subdomains.

	Ω_1	Ω_2	Ω_3
wave speed c	$1/4$	2	$1/2$
time grids Δt_i	13×10^{-2}	39×10^{-3}	1×10^{-1}

4.5 Discontinuous Wave Speed and Non-Matching Time Steps

To test the method on problems not covered by the theory, we now consider the wave equation with variable wave speed $\partial_{tt}u - (c(x))^2\partial_{xx}u = 0$, with homogeneous initial conditions and the Dirichlet boundary conditions $u(0,t) = t^2$, $u(6,t) = t^3$. We decompose the spatial domain $\Omega := (0,6)$ into three equal subdomains Ω_i, $i = 1,2,3$, and use a random initial guess to start the DNWR iteration. For the spatial discretization, we take a uniform mesh in space with mesh size $\Delta x = 1\times 10^{-1}$, and for the time discretization, we use the non-uniform time grids Δt_i, $i = 1,2,3$, as indicated in Table 4.2, together with the piece-wise constant wave speed. To transmit interface data between the non-matching time grids at interfaces, we use an optimal complexity projection algorithm that advances linearly along the interfaces like in merge sort, summing the integrals needed from the smaller mesh cells that contribute to the bigger ones in a finite volume sense; see [19, Section 4] for the complete algorithm in Matlab. For a generalization to higher dimensions and triangular and tetrahedral grids, see [17,18]. In Figure 4.7 (a) we show the non-uniform time steps for different subdomains. Figure 4.7 (b), (c) and (d) give the three-step convergence of the DNWR algorithm for $T = 2$ (Note that panel (c) seems to have already converged after two iterations, but measuring the error shows that there is still error at the order of 1e-5 left, which is eliminated in panel (d) after the third iteration).

5 Conclusions

We presented and studied a Dirichlet-Neumann Waveform Relaxation method for parabolic and hyperbolic problems and decompositions into many subdomains. We proved rigorous convergence estimates for the case of the heat and wave equation in 1D, which show that for parabolic problems, the algorithm converges superlinearly, and for hyperbolic problems in a finite number of steps. In both cases, convergence is faster when subdomains are larger, or time windows smaller. We also extended our analysis to the 2D wave equation case using Fourier techniques, and obtained again convergence in a finite number of steps. We compared the new algorithm to Neumann-Neumann and Schwarz Waveform Relaxation methods, which showed that it is competitive, and also tested the algorithm for non-constant wave speeds and non-

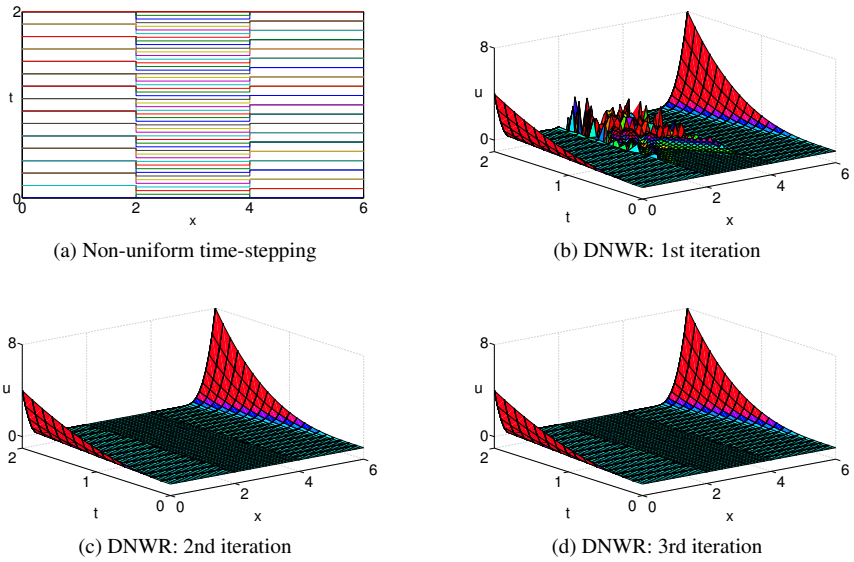

(a) Non-uniform time-stepping

(b) DNWR: 1st iteration

(c) DNWR: 2nd iteration

(d) DNWR: 3rd iteration

Fig. 4.7: Convergence of the DNWR method applied to the wave equation for non-uniform time steps for $\theta = 1/2$ for $T = 2$

matching time grids, a case not covered by our analysis. To introduce further time parallelism in this new algorithm, one should use a pipelining technique as described in [47].

Acknowledgements We thank the editors and the anonymous referees for their valuable and constructive comments, which greatly improved the quality of our paper.

A Appendix

For equal subdomains, with subdomain size h, we can deduce a better estimate:

$$\max_{1\le i\le 2m} \| w_i^k \|_{L^\infty(0,T)} \le \left(\min\{2m-1, Q(h,\nu,T)\}\right)^k \operatorname{erfc}\left(\frac{kh}{2\sqrt{\nu T}}\right) \max_{1\le i\le 2m} \| w_i^0 \|_{L^\infty(0,T)},$$

where $Q(h,\nu,T) := 2\operatorname{erfc}\left(\frac{h}{2\sqrt{\nu T}}\right) + \sum_{j=0}^{\infty} 2^{j+1}\operatorname{erfc}\left(\frac{jh}{2\sqrt{\nu T}}\right)$.

Here is an outline of the proof: For equal-length subdomains we have $h_i = h$ for $i = 1,\ldots,2m+1$, so that $\gamma_i = \gamma, \sigma_i = \sigma$ and $\gamma_{i,j} = 1, \sigma_{i,j} = 0$ for all i, j in (3.10). Therefore, we derive for $i = 1$ the recurrence

$$\begin{aligned}\hat{v}_1^k &= \frac{1}{\gamma}\hat{v}_1^{k-1} - \left(1-\frac{1}{\gamma^2}\right)\hat{v}_2^{k-1} - \cdots - \frac{1}{\gamma^{m-3}}\left(1-\frac{1}{\gamma^2}\right)\hat{v}_{m-1}^{k-1} - \frac{1}{\gamma^{m-2}}\hat{v}_m^{k-1} + \frac{1}{\gamma^{m-1}}\hat{v}_{m+1}^{k-1} \\ &=: \sum_{j=1}^{m+1} \hat{q}_j \hat{v}_j^{k-1}. \end{aligned} \tag{A.1}$$

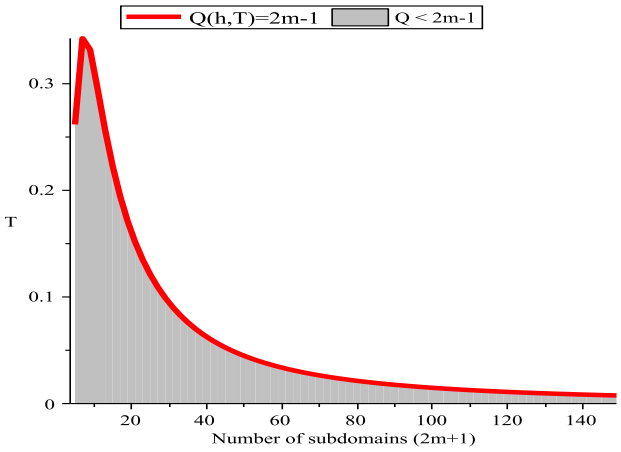

Fig. A.1: Comparison of the two estimates (A.2) and (A.4) for $\nu = 1$

The recurrence for other values of i can be deduced similarly. Note that the estimate from Theorem 2.1 also holds in this case with $h_{\max} = h_{m+1} = h$:

$$\max_{1\le i\le 2m} \| w_i^k \|_{L^\infty(0,T)} \le (2m-1)^k \operatorname{erfc}\left(\frac{kh}{2\sqrt{\nu T}}\right) \max_{1\le i\le 2m} \| w_i^0 \|_{L^\infty(0,T)} . \tag{A.2}$$

We now present a different estimate starting from (A.1). By back transforming into the time domain we obtain $v_1^k(t) = \sum_{j=1}^{m+1} \left(q_j * v_j^{k-1}\right)(t)$. Part 3 of Result 1 yields

$$\begin{aligned} \|v_1^k\|_{L^\infty(0,T)} &\le \sum_{j=1}^{m+1} \|v_j^{k-1}\|_{L^\infty(0,T)} \int_0^T |q_j(\tau)| d\tau \\ &\le \max_{1\le j\le m+1} \| v_j^{k-1} \|_{L^\infty(0,T)} \sum_{j=1}^{m+1} \int_0^T |q_j(\tau)| d\tau. \end{aligned} \tag{A.3}$$

Set $f_k(t) := \mathscr{L}^{-1}\left(\frac{1}{\gamma^k}\right)$. Since $\lim_{s\to 0+} \left|1 - \frac{1}{\gamma^2}\right| \le 2$, we have from (A.3)

$$\sum_{j=1}^{m+1} \int_0^T |q_j(\tau)| d\tau \le \int_0^T \left(f_1(t) + 2 + 2f_1(t) + \cdots + 2f_{m-3}(t) + f_{m-2}(t) + f_{m-1}(t)\right) dt.$$

Therefore using Lemma 3.3, we obtain

$$\sum_{j=1}^{m+1} \int_0^T |q_j(\tau)| d\tau \le 2\operatorname{erfc}\left(\frac{h}{2\sqrt{\nu T}}\right) + \sum_{j=0}^{m-1} 2^{j+1} \operatorname{erfc}\left(\frac{jh}{2\sqrt{\nu T}}\right) \le Q(h,\nu,T),$$

where $Q(h,\nu,T) := 2\operatorname{erfc}\left(\frac{h}{2\sqrt{\nu T}}\right) + \sum_{j=0}^{\infty} 2^{j+1} \operatorname{erfc}\left(\frac{jh}{2\sqrt{\nu T}}\right)$. So we get the second estimate as

$$\max_{1\le i\le 2m} \| w_i^k \|_{L^\infty(0,T)} \le Q^k \operatorname{erfc}\left(\frac{kh}{2\sqrt{\nu T}}\right) \max_{1\le i\le 2m} \| w_i^0 \|_{L^\infty(0,T)} . \tag{A.4}$$

The result follows combining the two estimates (A.2) and (A.4).

We compare the two estimates (A.2) and (A.4) in Figure A.1 for $\nu = 1$. The region below the red curve is where the estimate (A.2) is more accurate than (A.4).

References

1. Bennequin, D., Gander, M.J., Gouarin, L., Halpern, L.: Optimized Schwarz waveform relaxation for advection reaction diffusion equations in two dimensions. Numerische Mathematik **134**(3), 513–567 (2016)
2. Bennequin, D., Gander, M.J., Halpern, L.: A homographic best approximation problem with application to optimized Schwarz waveform relaxation. Math. Comp. **78**(265), 185–223 (2009). DOI 10.1090/S0025-5718-08-02145-5. URL http://dx.doi.org/10.1090/S0025-5718-08-02145-5
3. Bjørstad, P.E., Widlund, O.B.: Iterative methods for the solution of elliptic problems on regions partitioned into substructures. SIAM J. Numer. Anal. **23**(6), 1097–1120 (1986). DOI 10.1137/0723075. URL http://dx.doi.org/10.1137/0723075
4. Börgers, C.: The Neumann–Dirichlet domain decomposition method with inexact solvers on the subdomains. Numerische Mathematik **55**(2), 123–136 (1989)
5. Bourgat, J.F., Glowinski, R., Le Tallec, P., Vidrascu, M.: Variational formulation and algorithm for trace operator in domain decomposition calculations. In: Domain decomposition methods (Los Angeles, CA, 1988), pp. 3–16. SIAM, Philadelphia, PA (1989)
6. Bramble, J.H., Pasciak, J.E., Schatz, A.H.: An iterative method for elliptic problems on regions partitioned into substructures. Math. Comp. **46**(174), 361–369 (1986). DOI 10.2307/2007981. URL http://dx.doi.org/10.2307/2007981
7. Carlenzoli, C., Quarteroni, A.: Adaptive domain decomposition methods for advection-diffusion problems. In: Modeling, mesh generation, and adaptive numerical methods for partial differential equations, pp. 165–186. Springer (1995)
8. Claeys, X., Hiptmair, R.: Electromagnetic scattering at composite objects: a novel multi-trace boundary integral formulation. ESAIM: Mathematical Modelling and Numerical Analysis **46**(6), 1421–1445 (2012)
9. De Roeck, Y.H., Le Tallec, P.: Analysis and test of a local domain-decomposition preconditioner. In: Fourth International Symposium on Domain Decomposition Methods for Partial Differential Equations (Moscow, 1990), pp. 112–128. SIAM, Philadelphia, PA (1991)
10. Discacciati, M., Quarteroni, A.: Convergence analysis of a subdomain iterative method for the finite element approximation of the coupling of Stokes and Darcy equations. Computing and Visualization in Science **6**(2-3), 93–103 (2004)
11. Dolean, V., Gander, M.J.: Multitrace formulations and dirichlet-neumann algorithms. In: Domain decomposition methods in science and engineering XXII, pp. 147–155. Springer (2016)
12. Funaro, D., Quarteroni, A., Zanolli, P.: An iterative procedure with interface relaxation for domain decomposition methods. SIAM J. Numer. Anal. **25**(6), 1213–1236 (1988). DOI 10.1137/0725069. URL http://dx.doi.org/10.1137/0725069
13. Gander, M.J.: 50 years of time parallel time integration. In: Multiple Shooting and Time Domain Decomposition Methods, pp. 69–113. Springer (2015)
14. Gander, M.J., Halpern, L.: Absorbing Boundary Conditions for the Wave Equation and Parallel Computing. Math. Comp. **74**(249), 153–176 (2005). DOI 10.1090/S0025-5718-04-01635-7. URL http://dx.doi.org/10.1090/S0025-5718-04-01635-7
15. Gander, M.J., Halpern, L.: Optimized Schwarz Waveform Relaxation for Advection Reaction Diffusion Problems. SIAM J. Numer. Anal. **45**(2), 666–697 (2007). DOI 10.1137/050642137. URL http://dx.doi.org/10.1137/050642137
16. Gander, M.J., Halpern, L., Nataf, F.: Optimal Schwarz Waveform Relaxation for the One Dimensional Wave Equation. SIAM J. Numer. Anal. **41**(5), 1643–1681 (2003). DOI 10.1137/S003614290139559X. URL http://dx.doi.org/10.1137/S003614290139559X
17. Gander, M.J., Japhet, C.: An Algorithm for Non-Matching Grid Projections with Linear Complexity. In: M. Bercovier, M.J. Gander, D. Keyes, O. Widlund (eds.) Domain Decomposition in Science and Engineering XVIII (2008)
18. Gander, M.J., Japhet, C.: Algorithm 932: PANG: software for nonmatching grid projections in 2D and 3D with linear complexity. ACM Trans. Math. Software **40**(1), Art. 6, 25 (2013). DOI 10.1145/2513109.2513115. URL http://dx.doi.org/10.1145/2513109.2513115
19. Gander, M.J., Japhet, C., Maday, Y., Nataf, F.: A new cement to glue nonconforming grids with Robin interface conditions: the finite element case. In: Domain decomposition methods in science and engineering, pp. 259–266. Springer (2005)
20. Gander, M.J., Kwok, F., Mandal, B.C.: Dirichlet-Neumann and Neumann-Neumann Waveform Relaxation Algorithms for Parabolic Problems. Electron. Trans. Numer. Anal. **45**, 424–456 (2016)

21. Gander, M.J., Kwok, F., Mandal, B.C.: Dirichlet-Neumann and Neumann-Neumann Waveform Relaxation for the Wave Equation. In: T. Dickopf, M.J. Gander, L. Halpern, R. Krause, L. Pavarino (eds.) Domain Decomposition Methods in Science and Engineering XXII, Lecture Notes in Computational Science and Engineering, pp. 501–509. Springer International Publishing (2016). DOI 10.1007/978-3-319-18827-0_51. URL http://dx.doi.org/10.1007/978-3-319-18827-0_51
22. Gander, M.J., Stuart, A.M.: Space-time continuous analysis of waveform relaxation for the heat equation. SIAM J. Sci. Comput. **19**(6), 2014–2031 (1998). DOI 10.1137/S1064827596305337. URL http://dx.doi.org/10.1137/S1064827596305337
23. Gander, M.J., Zhao, H.: Overlapping Schwarz waveform relaxation for the heat equation in n dimensions. BIT **42**(4), 779–795 (2002). DOI 10.1023/A:1021900403785. URL http://dx.doi.org/10.1023/A:1021900403785
24. Giladi, E., Keller, H.: Space time domain decomposition for parabolic problems. Tech. Rep. 97-4, Center for research on parallel computation CRPC, Caltech (1997)
25. Gorb, Y., Kurzanova, D.: Heterogeneous domain decomposition method for high contrast dense composites. Journal of Computational and Applied Mathematics **337**, 135–149 (2018)
26. Hiptmair, R., Jerez-Hanckes, C.: Multiple traces boundary integral formulation for helmholtz transmission problems. Advances in Computational Mathematics **37**(1), 39–91 (2012). DOI 10.1007/s10444-011-9194-3. URL https://doi.org/10.1007/s10444-011-9194-3
27. Hoang, T.T.P.: Space-time domain decomposition methods for mixed formulations of flow and transport problems in porous media. Ph.D. thesis, University Paris 6, France (2013)
28. Hoang, T.T.P., Jaffré, J., Japhet, C., Kern, M., Roberts, J.E.: Space-time domain decomposition methods for diffusion problems in mixed formulations. SIAM Journal on Numerical Analysis **51**(6), 3532–3559 (2013)
29. Jiang, Y.L., Song, B.: Coupling parareal and dirichlet-neumann/neumann-neumann waveform relaxation methods for the heat equation. In: International Conference on Domain Decomposition Methods XXIV, pp. 405–413. Springer (2018)
30. Krause, R.H., Wohlmuth, B.I.: A Dirichlet–Neumann type algorithm for contact problems with friction. Computing and visualization in science **5**(3), 139–148 (2002)
31. Kwok, F.: Neumann-Neumann Waveform Relaxation for the Time-Dependent Heat Equation. In: J. Erhel, M.J. Gander, L. Halpern, G. Pichot, T. Sassi, O.B. Widlund (eds.) Domain Decomposition in Science and Engineering XXI, vol. 98, pp. 189–198. Springer-Verlag (2014)
32. Le Tallec, P., De Roeck, Y.H., Vidrascu, M.: Domain decomposition methods for large linearly elliptic three-dimensional problems. J. Comput. Appl. Math. **34**(1), 93–117 (1991). DOI 10.1016/0377-0427(91)90150-I. URL http://dx.doi.org/10.1016/0377-0427(91)90150-I
33. Lemarié, F., Debreu, L., Blayo, E.: Toward an optimized global-in-time schwarz algorithm for diffusion equations with discontinuous and spatially variable coefficients, part 1: the constant coefficients case. Electron. Trans. Numer. Anal **40**, 148–169 (2013)
34. Lemarié, F., Debreu, L., Blayo, E.: Toward an optimized global-in-time schwarz algorithm for diffusion equations with discontinuous and spatially variable coefficients, part 2: the variable coefficients case. Electron. Trans. Numer. Anal **40**, 170–186 (2013)
35. Maier, I., Haasdonk, B.: A Dirichlet–Neumann reduced basis method for homogeneous domain decomposition problems. Applied Numerical Mathematics **78**, 31–48 (2014)
36. Mandal, B.C.: Convergence Analysis of Substructuring Waveform Relaxation Methods for Space-time Problems and Their Application to Optimal Control Problems. Ph.D. thesis, University of Geneva (2014). URL http://archive-ouverte.unige.ch/unige:46146
37. Mandal, B.C.: A Time-Dependent Dirichlet-Neumann Method for the Heat Equation. In: J. Erhel, M.J. Gander, L. Halpern, G. Pichot, T. Sassi, O.B. Widlund (eds.) Domain Decomposition in Science and Engineering XXI, vol. 98, pp. 467–475. Springer-Verlag (2014)
38. Mandal, B.C.: Neumann-Neumann Waveform Relaxation Algorithm in Multiple Subdomains for Hyperbolic Problems in 1d and 2d. Numer. Methods Partial Differ. Equ. (2016). URL DOI10.1002/num.22112
39. Marini, L.D., Quarteroni, A.: An Iterative Procedure for Domain Decomposition Methods: a Finite Element Approach. SIAM, in Domain Decomposition Methods for PDEs, I pp. 129–143 (1988)
40. Marini, L.D., Quarteroni, A.: A relaxation procedure for domain decomposition methods using finite elements. Numer. Math. **55**(5), 575–598 (1989). DOI 10.1007/BF01398917. URL http://dx.doi.org/10.1007/BF01398917
41. Martini, I., Haasdonk, B.: Output error bounds for the Dirichlet–Neumann reduced basis method. In: Numerical Mathematics and Advanced Applications-ENUMATH 2013, pp. 437–445. Springer (2015)

42. Monge, A., Birken, P.: On the convergence rate of the Dirichlet–Neumann iteration for unsteady thermal fluid–structure interaction. Computational Mechanics **62**(3), 525–541 (2018)
43. Monge, A., Birken, P.: A multirate neumann–neumann waveform relaxation method for heterogeneous coupled heat equations. SIAM Journal on Scientific Computing **41**(5), S86–S105 (2019)
44. Monge, A., Birken, P.: A time-adaptive Dirichlet–Neumann waveform relaxation method for coupled heterogeneous heat equations. PAMM **19**(1) (2019)
45. Monge, A., Birken, P.: A time adaptive multirate neumann-neumann waveform relaxation method for thermal fluid-structure interaction. In: Domain Decomposition Methods in Science and Engineering XXV, p. to appear. Springer (2020)
46. Oberhettinger, F., Badii, L.: Tables of Laplace transforms. Springer-Verlag, New York-Heidelberg (1973)
47. Ong, B.W., Mandal, B.C.: Pipeline Implementations of Neumann–Neumann and Dirichlet–Neumann Waveform Relaxation Methods. to appear (arXiv:1605.08503)
48. Toselli, A., Widlund, O.: Domain decomposition methods—algorithms and theory, *Springer Series in Computational Mathematics*, vol. 34. Springer-Verlag, Berlin (2005). DOI 10.1007/b137868. URL http://dx.doi.org/10.1007/b137868